Journal of Inflammation Research

Dovepress
Taylor & Francis Group

Open Access Full Text Article

ORIGINAL RESEARCH

Mechanism of Lipi Jiangzhuo Decoction in Improving Metabolic Dysfunction-Associated Steatohepatitis Through the PERK/PINK1/GPx4 Pathway

Linlin Pan[1], Juhai Liu[1], Guowei Pang[2], Guirong Liu[1], Yuan Tian[3,4]

[1]College of Traditional Chinese Medicine, Shandong University of Traditional Chinese Medicine, Jinan City, Shandong Province, People's Republic of China; [2]Acupuncture and Moxibustion Massage College, Shandong University of Traditional Chinese Medicine, Jinan City, Shandong Province, People's Republic of China; [3]Foreign Languages College, Shandong University of Traditional Chinese Medicine, Jinan City, Shandong Province, People's Republic of China; [4]First Clinical Medical College, Shandong University of Traditional Chinese Medicine, Jinan City, Shandong Province, People's Republic of China

Correspondence: Yuan Tian, Foreign Languages College, Shandong University of Traditional Chinese Medicine, No. 4655, Daxue Road, Changqing District, Jinan City, Shandong Province, 250355, People's Republic of China, Tel +86-053189628253, Email tianyuan8612@163.com

Background: Metabolic dysfunction-associated steatohepatitis (MASH) is characterized primarily by hepatocyte lipoapoptosis and hepatic inflammation, frequently developing from overweight/obesity. To date, no specific therapeutics exist to reverse MASH. Although resmetirom has been approved in some regions, patients in many Asian countries, including China, still lack access to approved pharmacotherapy for MASH. Lipi Jiangzhuo decoction (LPJZD) is a promising traditional Chinese medicine formula for MASH. However, to date, there have been no comprehensive studies clarifying its potential mechanism of action. This study aims to elucidate the underlying mechanism of action of LPJZD in the treatment of MASH.

Materials and Methods: A MASH mouse model was established by feeding a high-fat diet and subjecting them to fatigue protocols and cold stress for 12 weeks. After treating MASH mice with LPJZD, biochemical assays were conducted to assess the efficacy of LPJZD in alleviating the MASH symptoms. In addition, the in vitro effects of LPJZD on MASH were evaluated using L-02 cells. Specifically, we analyzed the effect of LPJZD on endoplasmic reticulum (ER) stress, mitophagy, and ferroptosis by Western blot analysis, flow cytometry, immunofluorescence staining, and enzyme-linked immunosorbent assay.

Results: In vivo, LPJZD effectively improved the inflammatory response, reduced body weight and blood lipid levels, improved liver function, reduced liver lipid droplet accumulation, and ameliorated the pathological status of MASH mice. In vitro, LPJZD effectively inhibited ferroptosis by reducing ferrous ions and reactive oxygen species levels, increasing GPx4 protein expression, elevating glutathione levels, and ameliorating mitochondrial swelling and matrix thinning. Simultaneously, LPJZD activated mitophagy by increasing PINK1 and Parkin protein expression, augmenting mitophagosome number, and restoring mitochondrial membrane potential. Additionally, LPJZD suppressed ER stress by decreasing PERK protein expression. Notably, activation of ER stress using a PERK activator attenuated LPJZD's effects on mitophagy activation and ferroptosis inhibition, inhibition of mitophagy via a PINK1 inhibitor diminished LPJZD's anti-ferroptotic effect, and administration of a GPx4 inhibitor reduced LPJZD's suppression of ferroptosis. Therefore, these results demonstrate that LPJZD ameliorates MASH by regulating the PERK/PINK1/GPx4 pathway.

Conclusion: LPJZD can improve MASH by regulating ER stress-mitophagy -ferroptosis axis in liver cells. The role of LPJZD in anti-inflammatory therapy provides new insights for the clinical prevention and treatment of MASH.

Keywords: Lipi Jiangzhuo decoction, metabolic dysfunction-associated steatohepatitis, endoplasmic reticulum stress, mitophagy, ferroptosis

Received: 5 April 2025
Accepted: 29 July 2025
Published: 13 August 2025

Graphical Abstract

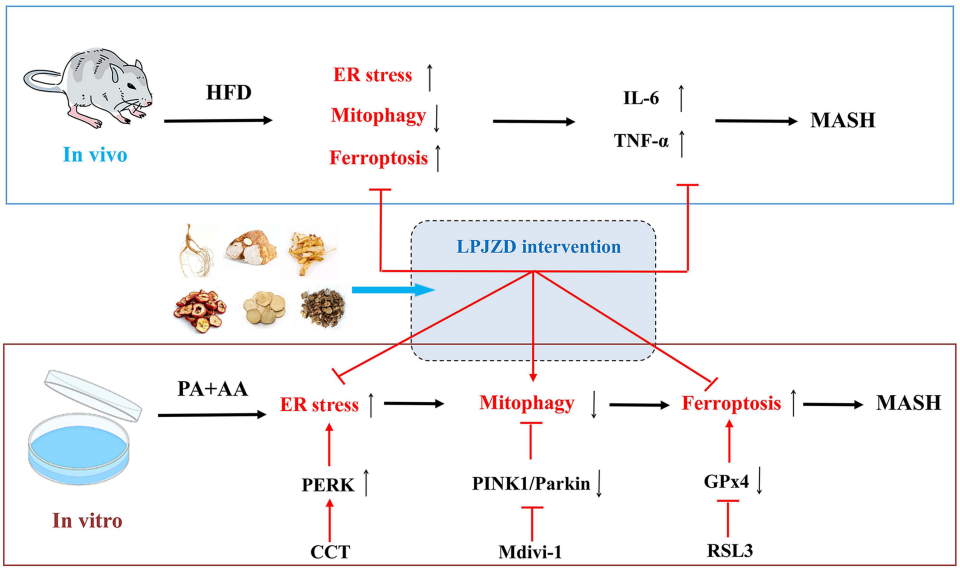

Introduction

Metabolic dysfunction-associated steatotic liver disease (MASLD), formerly known as non-alcoholic fatty liver disease (NAFLD), is a chronic, progressive, metabolically driven liver injury closely associated with insulin resistance and genetic susceptibility. Metabolic dysfunction-associated steatohepatitis (MASH) represents the critical inflection point for MASLD progression toward increased risk of adverse outcomes and is recognized as the pivotal stage in the development of MASLD-related cirrhosis and hepatocellular carcinoma.[1] This condition is a disease characterized by liver fat accumulation caused by non-alcoholic factors, and characterized primarily by hepatic cell apoptosis and inflammation. Currently, the incidence rate of MAFLD is estimated to be about 25% of the global population, and about 20–30% of the patients will develop into MASH.[2] A recent study predicts that the prevalence of MAFLD in China will grow at the highest rate globally, with an estimated 314 million cases by 2029.[3] MASLD is also closely associated with the development and progression of diabetes mellitus, cardiovascular disease, and chronic kidney disease. Among MASLD patients, 55% present with type 2 diabetes mellitus.[4,5] Furthermore, MASLD constitutes an independent risk factor for cardiovascular disease, accounting for 40%-50%.[6] The primary pathogenesis of MASH is not yet fully understood, and areas of concern and research in the academic community include steatosis, iron overload, endoplasmic reticulum (ER) stress, and mitochondrial dysfunction. Not until March 2024 did the US Food and Drug Administration approve resmetirom as the world's first and currently only medication for MASH.[7,8] However, resmetirom has not yet been marketed in China and lacks clinical evidence in Asian populations. Consequently, the vast majority of MASH patients in China still lack access to approved pharmacotherapy. Therefore, it is extremely important to fully understand the pathogenesis of MASH and investigate new potential drugs to treat the progression of MASH, in order to prevent the disease from developing into late stage liver cirrhosis and even cancer.

Recent studies have shown that ER stress leads to the production of transcription factors and kinases, which can exacerbate mitophagy dysfunction and affect lipid homeostasis in liver cells. Therefore, new ideas for improving MASH can be gained from the dialogue between the endoplasmic reticulum and mitochondria to control the severe development of MASH.[9] Protein kinase R-like endoplasmic reticulum kinase (PERK) is involved in the early response to ER stress. Activated PERK regulates cellular autophagy and dynamic mitochondrial changes. Therefore, activated PERK can connect mitochondria to the endoplasmic reticulum.[10] Mitochondrial homeostasis can be regulated by removing impaired mitochondria through mitophagy, and as a result PINK1/Parkin-mediated mitophagy is currently one of the most widely

studied and in-depth mechanisms of mitophagy. Studies have shown that inhibiting parkin-mediated mitophagy in mouse liver can lead to hepatic steatosis and exacerbate the progression of MAFLD.[11] In addition, recent studies have found that ferroptosis can exacerbate inflammation, oxidative stress, and cell damage, and is an important pathological mechanism for the development of MASH.[12] Also, PINK1/Parkin mediated mitophagy can effectively inhibit ferroptosis.[13] Therefore, inhibiting ER stress, activating mitophagy, and inhibiting ferroptosis are important strategies for the treatment of MASH.

The remarkable efficacy of traditional Chinese medicine (TCM) has been corroborated for thousands of years. The Lipi Jiangzhuo decoction (LPJZD) is an effective TCM formula that has been used to treat MAFLD.[14] LPJZD is composed of six Chinese herbs, namely Huangjing, Gegen, Renshen, Cangzhu, Shanzha, and Zexie. An ancient Chinese medicine book, *The Records of Famous Doctors* (Chinese name: *Mingyi Bielu*), described that Gegen and Huangjing can nourish yin qi, generate body fluid, and in combination with Renshen can balance yin and yang. Cangzhu can invigorate the spleen and dispel dampness, Zexie can clear dampness and promote diuresis, and Shanzha can support digestion and promote qi. The reconciliation of various herbs can clear obstacles for spleen transportation and transformation, thereby regulating lipid metabolism.

The effect of LPJZD on lipid metabolism has been verified in previous clinical and animal studies. Liu et al found that LPJZD significantly improved blood lipid levels and hemorheological indexes in patients with dyslipidemia, and downregulated the ApoB/ApoA-I ratio.[15] Yan et al found that LPJZD can increase the expression of ApoE mRNA in the liver of dyslipidemic rats, and reduce the expression of ApoC-III mRNA in blood, which in effect regulate lipid metabolism.[16] Metabolomics studies have revealed that the LPJZD is involved in multiple metabolic pathways, such as the tricarboxylic acid cycle, amino acid metabolism, and energy metabolism, by regulating the expression of metabolites such as citric acid, leucine, valine, and creatine in rat serum,[17] and these metabolites have been shown to have a significant effect on improving MASH.[18,19] There are also studies indicating that the main compounds of LPJZD, namely quercetin, arginine, naringenin, and berberine, have the effect of regulating ER stress, mitophagy, and ferroptosis. For example, quercetin and berberine have been shown to alleviate ER stress, activate mitophagy, and inhibit cell ferroptosis.[20–25] Arginine and naringenin have been demonstrated to alleviate ER stress and inhibit cell ferroptosis.[26–29] Therefore, based on previous experimental findings, we hypothesize that LPJZD can alleviate ER stress, activate mitophagy, inhibit the occurrence of cell ferroptosis, and ultimately improve MASH. Therefore, in this study we investigated the effects of LPJZD on ER stress, mitophagy, and ferroptosis in MASH using in vivo and in vitro models. This study aims to elucidate the molecular mechanism by which LPJZD improves MASH, provide a scientific basis for its clinical application in the treatment of MASH, and promote the modernization research of TCM formulas.

Materials and Methods

Ethical Approval

This study was approved by the Animal Ethics Committee of Shandong University of Traditional Chinese Medicine with the permit number: SDUTCM20220707005, all animal experiments confirmed to the Guide for the Care and Use of Laboratory Animals.

Decoction and Drug

The contents of LPJZD were shown in Table 1, and the raw herb materials were purchased from Beijing Tongrentang Co. Ltd. (Beijing, China). Renshen, Huangjing, Cangzhu, Shanzha, Gegen, and Zexie were mixed at a fixed ratio of 2:5:5:5:10:10 in a round-bottomed flask and then dissolved in 10 times total drug weight water and allowed to soak for 12 h. Subsequently, after heating the mixture to reflux for 1 h, the first solution was extracted and filtered. Then, after adding the same amount of water to the residue and heating to reflux for 1 h, the second solution was extracted and combined with the first filtered solution. Ultimately, the solution was concentrated using a rotary evaporator at 50°C to obtain the LPJZD extract (2g/mL). Obeticholic acid (OCA; Bide Pharmaceutical Technology Co., Ltd., Shanghai, China) was used as a positive control drug, at a dose of 30 mg/kg/d for in vivo animal experiments according to a previous report.[30]

Table 1 Contents of LPJZD

Chinese name	Latin name	Medicinal part [a]	Weight (g)
Huangjing	*Polygonatum sibiricum* F.Delaroche	Root	15
Gegen	*Pueraria alopecuroides* Craib	Root	30
Renshen	*Panax Ginseng* C. A. Mey	Root	6
Cangzhu	*Atractylodes lancea* (Thunb.) DC.	Rhizome	15
Shanzha	*Crataegus pinnatifida* Bunge	Fructus	15
Zexie	*Alisma plantago-aquatica* L.	Rhizome	30

Notes: [a]Renshen (batch number: 20200905, source: Jilin, China), Huangjing (batch number: 20201106, source: Shanxi, China), Cangzhu (batch number: 20201012, source: Sichuan, China), Shanzha (batch number: 20190902, source: Shandong, China), Gegen (batch number: 20190622, source: Zhejiang, China), and Zexie (batch number: 20191202, source: Fujian, China).

Serum samples from LPJZD-treated and untreated control mice were prepared as follows. Twenty eight-week-old C57BL/6J male mice were randomly divided into two groups (LPJZD-treated group and untreated control groups) using the random number table method. The mice in the treatment group received the optimal dose of LPJZD for MASH treatment by gavage, while the control group mice received an equal volume of physiological saline by gavage. After 1 week, the mice were anesthetized and 5 mL samples of whole blood were collected, and centrifuged at 3,000 rmp for 10 min. Afterwards, the supernatant from each sample was collected in separate centrifuge tubes, inactivated in a 56 °C water bath for 30 min, and eventually filtered and sterilized. Finally, the serum samples from LPJZD-treated mice and control mice were obtained, and stored them at −20 °C.

A Q-Orbitrap high-resolution liquid chromatography-mass spectrometry (LC-MS) system (Q Exactive™Plus, Thermo Fisher Scientific Inc., Waltham, MA, USA), coupled with electrospray ionization, was used to identify the compounds in LPJZD. The chromatographic analysis was performed using UltiMate 3000 RS column (100×2.1 mm, 1.8 um; Thermo Fisher Scientific Inc., Waltham, MA, USA). Solvents A (0.1% formic acid in aqueous, v/v) and solvent B (0.1% formic acid in acetonitrile, v/v) were used at a flow rate of 0.3 mL/min at 35 °C. Gradient elution conditions were performed as follows: 0–1 min at 2% B; 2–7 min at 2–20% B; 8–13 min at 20–50% B; 14–19 min at 50–80% B; 20–25 min at 80–95% B; 26–31 min at 95% B; and 32–37 min at 2% B. Mass spectrometry analysis employed both positive and negative electrospray ionization (ESI), with the following specific parameters: in positive ion mode, the spray voltage was set at 3.8 kV, capillary voltage at 2.5 kV, desolvation gas temperature and flow rate at 350°C and 800 L/h, and ESI source temperature at 110°C; In negative ion mode, the spray voltage was 3.5 kV, capillary voltage 2.0 kV, desolvation gas temperature and flow rate at 350°C and 600 L/h, with the ESI source temperature maintained at 110°C. Automatic calibration across m/z 150–2000 was performed in full-scan mode. Finally, the data were analyzed using the mzCloud (https://www.mzcloud.org/), mzVault (https://mytracefinder.com/), and ChemSpider (https://www.chemspider.com/) databases to identify the compounds present in LPJZD.

Animal Preparation

Eight-week-old male C57BL/6 mice (Weitong Lihua Experimental Animal Breeding Co. Ltd., Beijing, China; certificate no. SCXK2022-0005) with a body weight of 20 ± 2 g were housed under specific pathogen-free conditions. Briefly, mice fed a regular diet and ad libitum access to water were maintained at 23–25 °C, 50–60% relative humidity, and a 12–12 h light-dark cycle for one week. Then, the mice were randomly divided into a control group (n = 10) fed a normal diet, a MASH model group fed a high-fat diet consisting of fat emulsion (cholesterol 10 g, lard 20 g, sodium cholate 2 g, propylthiouracil 1 g, Tween-80 20 mL, propylene glycol 30 mL) and subjected to fatigue protocols and cold stress for 12 weeks.[31]

Ten mice were randomly selected to measure blood lipid levels, liver function, and inflammatory factor levels using the corresponding assays and reagents (Abcam, Cambridge, the United Kingdom) to verify the successful induction of MASH. Subsequently, the MASH mice on the high-fat diet were randomly subdivided into three groups of 10 mice each using the random number table method: the MASH model group, LPJZD group, and OCA group. The control group mice

were fed a standard diet, whereas the model group, LPJZD group, and OCA group were fed a high-fat diet. Over the same period, mice in the control and model groups received 0.5 mL/100 g/d of saline, while mice in the LPJZD group received LPJZD 12 g/kg/d by oral gavage, and those in the OCA group received OCA 30 mg/kg/d by oral gavage for 4 weeks.

Cell Preparation

The in vitro MASH cell model was established using L-02 cells (Shangen Biotechnology Co., Ltd., Wuhan, China) with palmitic acid (PA) and arachidonic acid (AA). The processing method of each group in the cell experiment was as follows: the control group cells were cultured in Dulbecco's modified Eagle medium (DMEM) containing 0.5% bovine serum albumin (BSA), the model group cells were cultured with PA and AA for 24 h. The LPJZD group cells were cultured with PA and AA, and then treated with LPJZD-containing serum for 24 h. The CCT020312 (CCT, activator of PERK) group cells were cultured with PA and AA, and then treated with CCT-containing serum for 24 h. The mdivi-1 (inhibitor of mitophagy) group cells were cultured with PA and AA, and then treated with mdivi-1-containing serum for 24 h. The RSL3 (inhibitor of GPx4) group cells were cultured with PA and AA, and then treated with RSL3-containing serum for 24 h.

Biochemical Analysis

After treatment with LPJZD for 4 weeks, the mice were euthanized, 1 mL of blood was collected from the abdominal aorta, and the serum was separated by centrifugation at 3,000 rpm for 15 min using a high-speed centrifuge (MilliporeSigma, Darmstadt, Germany). Ultimately, the serum samples were used to measure the levels of total cholesterol (TC), triglyceride (TG), low-density lipoprotein cholesterol (LDL-c), high-density lipoprotein cholesterol (HDL-c), alanine aminotransferase (ALT), aspartate aminotransferase (AST), malondialdehyde (MDA), superoxide dismutase (SOD), interleukin 6 (IL-6), and tumor necrosis factor-alpha (TNF-α) using the corresponding reagents (Nanjing Jiancheng Biotechnology Reagent Company, Nanjing, China).

Hematoxylin and Eosin Staining

The liver tissues were fixed with 4% paraformaldehyde, and then embedded in paraffin and sliced into 5 μm thick sections. The sections were dehydrated with ethanol and xylol followed by washing and staining of cell nuclei with 5% hematoxylin solution for 10 min. Then, the samples were incubated in a solution of HCl-ethanol for 30s, and counter-stained with eosin solution for 2 min. Finally, after staining the sections with hematoxylin and eosin (H&E), morphological examination was performed using a BX-53 light microscope (Olympus Corporation, Tokyo, Japan).

Oil -Red -O Staining

First, in dry liver tissue sections were placed in 10% formalin for 10 min. After washing three times with distilled water, the tissue sections were transferred to 100% propylene glycol for 5 min. Afterwards, the sections were heated at 60 °C and stained with preheated 0.5% oil-red-O dye (Beyotime Biotechnology, Shanghai, China) for 10 min. Then, the tissue sections were washed three times with 85% propylene glycol and distilled water, for 5 min each time. Finally, 2 mL of phosphate-buffered saline (PBS) was added and the slides were observed under a light microscope to visualize the formation of lipid droplets.

Immunofluorescence Assay Analysis

Cells were fixed with 4% paraformaldehyde, and permeabilized with 0.1% Triton X-100 (MilliporeSigma, Darmstadt, Germany) for 30 min. The slides were first incubated with the corresponding primary antibody (Abcam, Cambridge, the United Kingdom), and then with the appropriate secondary antibody, either goat anti-rabbit IgG (H&L) or goat anti-mouse IgG (H&L) (Abcam, Cambridge, the United Kingdom). Subsequently, the nuclei were stained with 1μg/mL 4',6-diamidino-2-phenylindole (DAPI; Beyotime Biotechnology, Shanghai, China). Finally, the slides were sealed, and images were captured under a fluorescence microscope (BX-51M, Olympus Corporation, Tokyo, Japan).

Methyl Thiazole Tetrazolium (MTT) Assay

The effects of different concentrations of LPJZD-treated serum, CCT, mdivi-1, and RSL3 on the cell survival rate were evaluated using the MTT assay. L-02 cells treated with PA and AA were seeded into a 96-well plate, with 2,500 cells per well (200 μL). Different concentrations of LPJZD-treated serum, as well as corresponding concentrations of CCT, RSL3, and mdivi-1 were added to the culture medium in sequence. Five wells were used for each group. A total of 20 μL of MTT solution (Yuanye Biotechnology Co., Ltd., Shanghai, China) was added to each well containing the treated cells and the plates were then incubated for 4 h. Then, 150 μL dimethyl sulfoxide (DMSO; MilliporeSigma, Darmstadt, Germany) was added to dissolve the formazan crystals for 10 min. Finally, the optical density (OD) value of the formazan solution was measured at the wavelength of 570 nm, and the OD values were used to calculate the cell viability.

Ferrous Ion Assay

After culturing cells for 24 h, cells from each group were collected after digestion with trypsin. The FeRhoNoxTM-1 dye probe (GC901; Goryo Chemical, Sapporo, Japan), kept at room temperature before use was used to measure ferrous ion (Fe^{2+}) levels. The corresponding amount of sterile DMSO was added to each probe box to obtain a final concentration of 1 mM. After removing the old culture medium from each well of the six-well plate, and washing twice with Hank's Balanced Salt Solution (HBSS; Thermo Fisher Scientific Inc., Waltham, MA, USA), an appropriate amount of FeRhoNoxTM-1 probe was added to each well to obtain a final concentration of 5 μM. Then, the cells were incubated in a 5% CO_2 incubator at 37 °C for 60 min, subsequently washed three times with HBSS, and observed under a fluorescence microscope (BX-51M, Olympus Corporation, Tokyo, Japan).

Reactive Oxygen Species Assay

A reactive oxygen species (ROS) detection kit (Nanjing Jiancheng Biotechnology Reagent Company, Nanjing, China) was used to measure the level of ROS. Cells were incubated with dichloro-dihydro-fluorescein diacetate (DCFH-DA; MilliporeSigma, Darmstadt, Germany) at a final concentration of 10 nM in the dark at 37 °C for 30 min. Then, after washing three times with PBS, the cells were collected and resuspended in PBS. Intracellular ROS levels were measured using flow cytometry (Beckman-Coulter, Brea, CA, USA) and data were analyzed using the FlowJo software (BD Biosciences, San Jose, CA, USA).

Glutathione Assay

Cells were seeded into six-well cell culture plates at a density of 1×10^6 cells/well and subjected to the corresponding treatment. After the treatments, the cells were detached by digestion with trypsin, collected by centrifugation, and used to measure intracellular glutathione (GSH) levels using a GSH detection kit (Nanjing Jiancheng Biotechnology Reagent Company, Nanjing, China) according to the manufacturer's instructions.

Mitochondrial Membrane Potential Assay

Mitochondrial membrane potential was measured using a fluorescent indicator JC-1 kit (Beyotime Biotechnology, Shanghai, China). An appropriate dilution of the JC-1 staining solution was prepared by adding 4 mL of distilled water to every 1 mL of JC-1 staining buffer. Then, the collected cells were incubated in JC-1 staining solution at 37 °C for 20 min in a 5% CO_2 incubator. Subsequently, the cells were washed twice with PBS and resuspended in cold PBS before being analyzed by flow cytometry.

Mitochondrial Morphology and Autophagosomes Assay

Cells were seeded at a density of 1×10^6 cells per well on a six-well plate and subjected to the corresponding treatment. After 24 h of drug treatment, the cells were detached and collected by centrifugation. Afterwards, cells were fixed at room temperature for 30 min using an electron microscope fixative. The cells were then dehydrated, embedded, cut into thin slices, and stained overnight at 4 °C. Morphological changes of mitochondria were observed and the number of

autophagosomes was counted using a transmission electron microscope (Talos™F200C, Thermo Fisher Scientific Inc., Waltham, MA, USA).

Cell Apoptosis Assay

After culturing the cells for 24 h, the cell culture medium was discarded and cells were detached by digestion with trypsin in EDTA free trypsin cell digestion medium. Subsequently, after collecting the detached cells by centrifugation at 1,000 rpm for 5 min, the supernatant was discarded and cells were washed once with PBS at 1,000 rpm for 5 min. After discarding the PBS, the cells were resuspended in a 1×binding buffer solution to a final cell concentration of 1×10^6 cells/mL. Then, a 100-μL cell suspension aliquot was transferred to a new tube, mixed with 5 μL of an Annexin V-fluorescein isothiocyanate solution and 10 μL of a propidium iodide solution (Keygen Biotechnology Co., Ltd., Nanjing, China), and incubated in the dark for 15 min. Finally, 300 μL of Annexin V-APC binding solution was added to the mixture and fluorescence was detected at a wavelength of 488 nm using a flow cytometer.

Western Blot Analysis

The liver tissue was pulverized, homogenized and then lysed using a radio immunoprecipitation assay (RIPA) buffer. After centrifuging the lysate at 12,000 rpm for 10 min, the protein concentration in the supernatant was measured using the bicinchoninic acid (BCA) assay quantification kit (Beyotime Biotechnology, Shanghai, China). Proteins were separated by sodium dodecyl sulfate-polyacrylamide gel electrophoresis (SDS-PAGE), and the separated proteins were transferred to a 0.45-μm pore-sized polyvinylidene fluoride membrane. Subsequently, the membranes were blocked with 2.5% non-fat dry milk in Tris-buffered saline with 0.1% Tween 20 (TBST) for 1 h and then incubated with the corresponding primary antibody (rabbit monoclonal, 1:1,000; Abcam, Cambridge, the United Kingdom) overnight at 4 °C. After washing four times with TBST, the membranes were incubated with the appropriate secondary antibody (anti-rabbit IgG 1:3,000) for 1 h. Immunoreactive proteins were ultimately visualized using an enhanced chemiluminescence Western Blotting analysis system (ProteinSimple, San Francisco, California, USA), and the results were analyzed using the LI-COR Odyssey Imaging System (LI-COR Biotech, Lincoln, NE, USA).

Statistical Analysis

SPSS software (IBM Corporation, Armonk, NY, USA) was used for statistical analysis, and the data were expressed as mean ± standard deviation (SD). One-way analysis of variance (ANOVA) was used to perform comparisons among groups, and a *T* test was used to perform comparisons between two groups. Differences were considered statistically significant at $P < 0.05$.

Results

Compound Analysis Based on LC-MS

The results of the analysis of the chemical compounds in LPJZD using Q-Orbitrap high-resolution LC-MS revealed 531 compounds that were matched in mzCloud, mzVault, and ChemSpider (Figure 1 and Supplementary file 1). The comprehensive score of 35 compounds in the mzCloud best match was greater than 90 (Table 2).

LPJZD Attenuates MASH in Mouse

To examine the effects of LPJZD on MASH in vivo, we determined changes in a series of biochemical indicators related to MASH in each group. The results revealed that, compared with the control group, the body weight of mice in the model group was significantly increased ($P<0.01$), the body weights of mice in LPJZD and OCA groups were significantly decreased after treatment compared with the model group ($P < 0.01$) (Figure 2A). Also, compared with the control group, the liver weight of mice in the model group was significantly increased ($P<0.01$), the liver weights of mice in the LPJZD and OCA groups were decreased significantly after treatment compared with the model group ($P < 0.01$) (Figure 2B). The ratio of liver weight to body weight (liver organ coefficient) indirectly reflects the lipid accumulation in the liver. Compared with the control group, the liver organ coefficient of mice in the model group

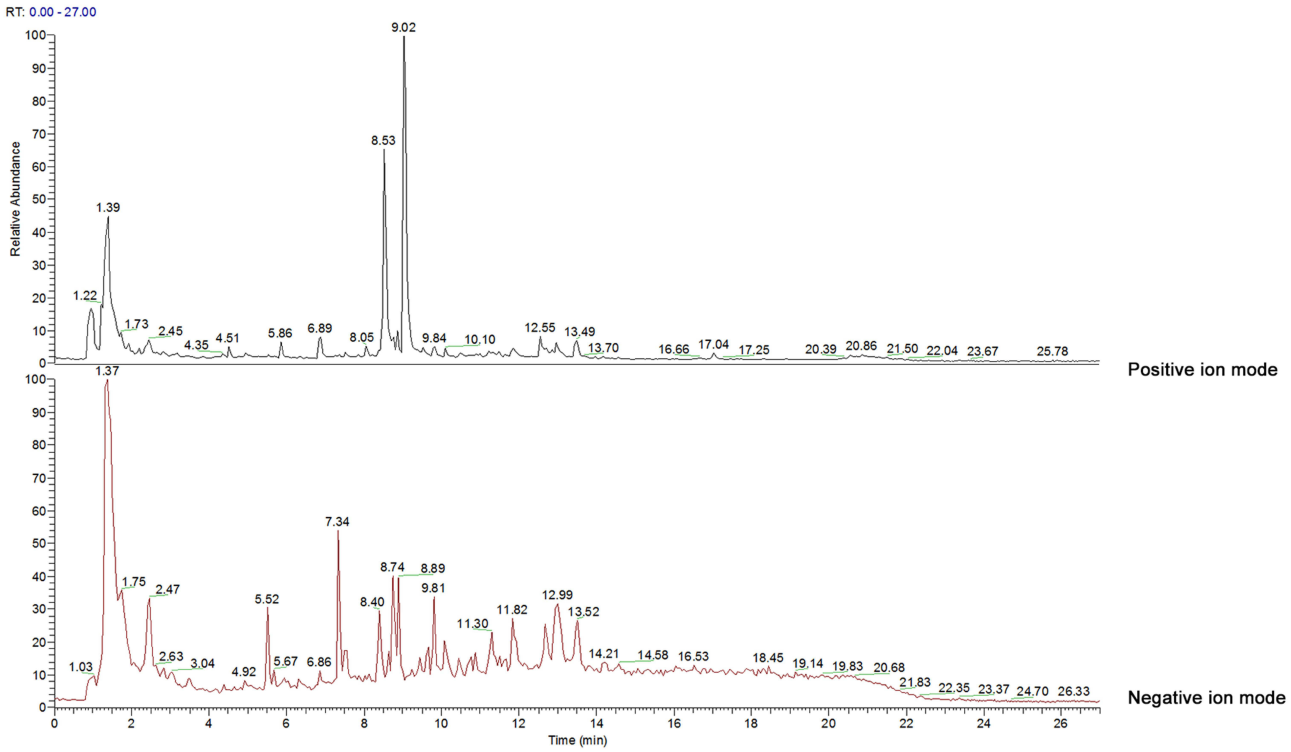

Figure 1 Identification of chemical compounds in the LPJZD.

was significantly increased (P<0.01), and the liver organ coefficients of the LPJZD and OCA groups were significantly lower than that of the model group ($P < 0.01$) (Figure 2C). These results indicate that LPJZD can decrease the body weight, liver weight, and liver organ coefficient in mice with MASH.

Table 2 The Main Chemical Compounds of LPJZD Matched in mzCloud, mzVault, and ChemSpider

Name	Formula	Molecular Weight	RT [min]	Chem Spider	mzCloud	mzVault	mzCloud Best Match
L-Phenylalanine	C9 H11 N O2	148.052	4.508	33	4	4	98.0
DL-Tryptophan	C11 H12 N2 O2	204.089	5.869	30	3	3	96.5
L-Tyrosine	C9 H11 N O3	164.047	2.464	45	2	2	96.5
Adenosine	C10 H13 N5 O4	267.096	3.172	33	2	2	95.7
2,3,4,9-Tetrahydro-1H-β-carboline-3-carboxylic acid	C12 H12 N2 O2	216.089	6.901	28	1	0	95.5
18-β-Glycyrrhetinic acid	C30 H46 O4	470.338	12.857	8	2	1	95.4
Isoliquiritigenin	C15 H12 O4	256.073	9.855	36	6	2	95.4
Catechin	C15 H14 O6	290.078	7.886	24	3	2	95.2
α-Aspartylphenylalanine	C13 H16 N2 O5	280.106	5.808	6	1	1	95.1
Bis(4-ethylbenzylidene)sorbitol	C24 H30 O6	414.203	14.549	10	2	0	95.0
Coumarin	C9 H6 O2	146.036	10.444	14	2	2	94.4
6-Gingerol	C17 H26 O4	276.172	13.661	18	6	0	94.3
Oleanolic acid	C30 H48 O3	438.349	11.874	5	2	0	94.2
N,N'-Dicyclohexylurea	C13 H24 N2 O	224.188	13.162	8	1	1	94.0
Formononetin	C16 H12 O4	268.073	12.564	31	2	2	93.7
Rutin	C27 H30 O16	610.152	8.668	18	2	1	93.2
Guanine	C5 H5 N5 O	134.023	4.368	4	2	2	93.0
Dipropyleneglycol dibenzoate	C20 H22 O5	342.146	16.632	12	2	2	92.8
Bis(2-ethylhexyl) phthalate	C24 H38 O4	390.276	22.756	21	6	4	92.6
DL-Arginine	C6 H14 N4 O2	157.085	1.218	5	2	2	92.5

(*Continued*)

Table 2 (Continued).

Name	Formula	Molecular Weight	RT [min]	Chem Spider	mzCloud	mzVault	mzCloud Best Match
Ferulic acid	C10 H10 O4	194.058	7.536	58	6	2	91.7
Berberine	C20 H17 N O4	335.114	9.049	1	4	1	91.6
Trigonelline	C7 H7 N O2	137.047	1.398	49	9	6	91.5
Adenosine 3'5'-cyclic monophosphate	C10 H12 N5 O6 P	329.052	4.935	11	1	1	91.4
3'-Adenosine monophosphate	C10 H14 N5 O7 P	347.062	3.160	16	3	2	91.2
DL-Glutamine	C5 H10 N2 O3	129.042	1.252	29	3	3	91.2
Hexadecanamide	C16 H33 N O	255.256	19.190	4	2	2	91.0
Nicotinamide	C6 H6 N2 O	122.048	1.939	16	1	1	90.7
2'-Deoxyadenosine	C10 H13 N5 O3	251.102	3.431	21	2	2	90.5
Daidzein	C15 H10 O4	254.057	10.399	30	1	1	90.5
Genistein	C15 H10 O5	270.052	11.723	0	1	0	90.4
L-Norleucine	C6 H13 N O2	131.095	2.341	58	10	10	90.3
Stearamide	C18 H37 N O	283.287	21.205	3	2	0	90.2
Quercetin	C15 H10 O7	302.042	9.254	15	8	4	90.1
Naringenin	C15 H12 O5	272.068	8.739	46	5	2	90.0

The results of the analyses of serum samples showed that, compared with the control group, the ALT and AST levels of mice in the model group were significantly increased ($P<0.01$), while the levels of these indicators were significantly decreased in the LPJZD and OCA groups ($P< 0.01$) (Figure 2D and E). The results for the blood lipids showed that, compared with the control group, the TC, TG, and LDL-c levels of mice in the model group were significantly increased ($P<0.01$), and the HDL-c level in the model group was significantly decreased ($P<0.01$), while the TC, TG, LDL-c, and HDL-c levels were significantly improved in the LPJZD and OCA groups compared with the model group ($P < 0.01$) (Figure 2F–I). In addition, compared with the control group, the MDA, IL-6, and TNF-α levels of mice in the model group were significantly increased ($P<0.01$), and the SOD level in the model group was significantly decreased ($P<0.01$), while the levels of MDA, SOD, IL-6, and TNF-α in the LPJZD and OCA groups were significantly improved after treatment compared with the model group ($P < 0.01$) (Figure 2J–M). These results suggest that LPJZD can improve the liver function, blood lipids, and inflammatory factors levels in mice with MASH.

H&E staining revealed that in the control group, the liver sections had clear hepatic lobule structures, the boundary of the portal area was clear, and the hepatocytes were radially distributed around the central vein. In contrast, in the model group, the liver sections exhibited hepatocyte swelling and lipid droplets, and vacuoles were present in the cytoplasm. In addition, compared with the model group, the arrangement of hepatocytes in the LPJZD and OCA groups tended to be normal, and the morphology of cell edema and vacuole changed, indicating that in these two groups, there was an obvious protective effect on liver tissue damage in MASH mice (Figure 2N). Oil-red-O staining showed no red lipid droplets in the liver tissue of the control group, whereas a large number of red lipid droplets were present in the liver tissue of the model group. Red lipid droplets were also observed in the LPJZD and OCA groups, but their number and degree were lower than those in the model group, especially in the LPJZD group. Therefore, LPJZD can reduce liver lipid droplet accumulation and improve the pathological status of MASH mice (Figure 2O).

LPJZD Induces Mitophagy, and Inhibits ER Stress and Ferroptosis

In this study, we detected changes in the expression level of the PERK protein, which is closely associated with ER stress (Figure 3A and B). The results showed that, compared with the control group, the protein level of PERK in the model group was significantly increased ($P<0.01$). Also, compared with the model group, the protein level of PERK in the LPJZD group was significantly decreased ($P<0.01$), indicating that LPJZD can inhibit the expression of key protein involved in ER stress. We also detected changes in expression levels of the proteins PINK1 and Parkin, which are closely related to mitophagy (Figure 3A–D). The results revealed that, compared with the control group, the protein expression levels of PINK1 and Parkin in the model group were significantly decreased ($P<0.01$). Compared with the model group,

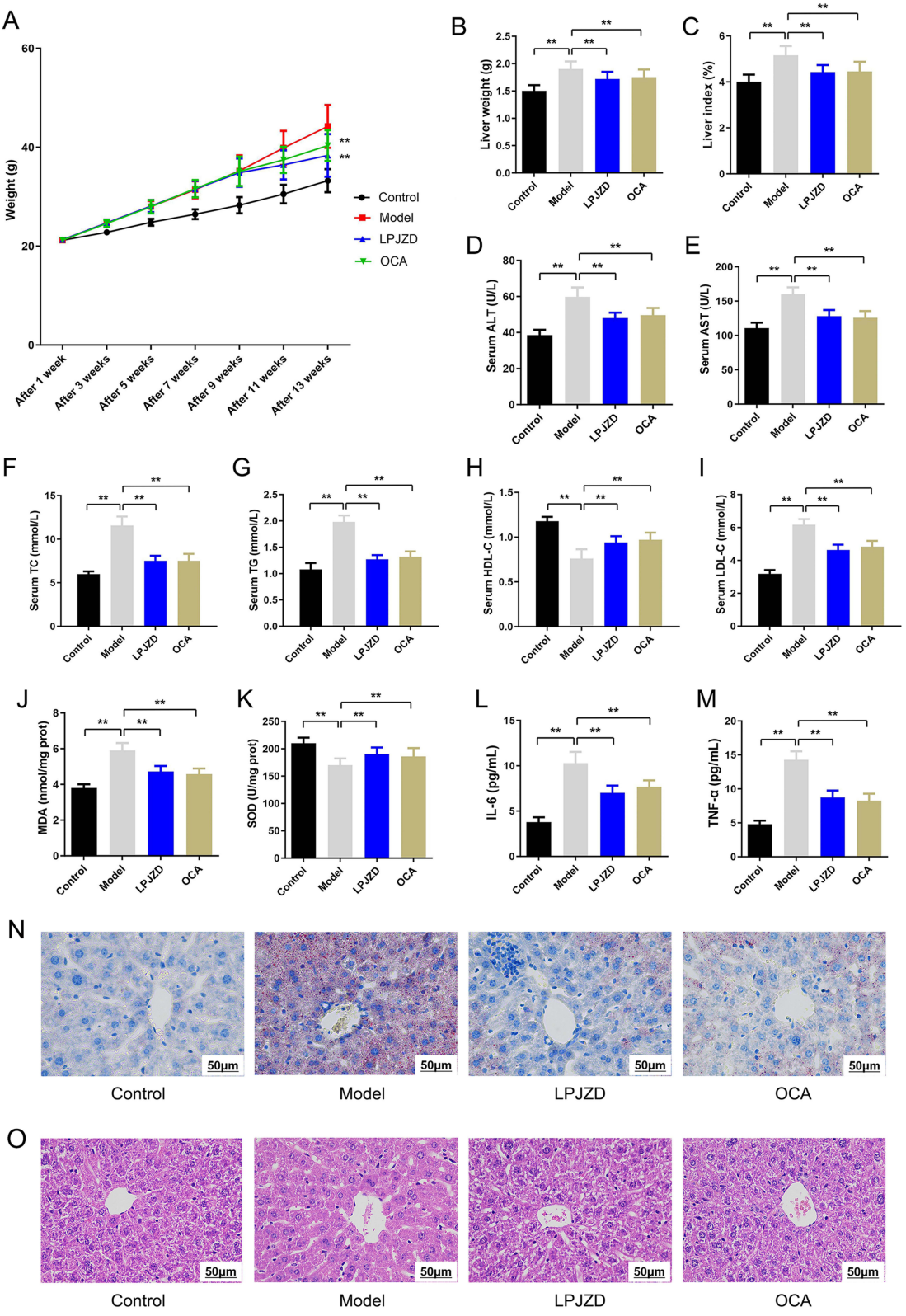

Figure 2 Effects of LPJZD on inflammatory response in the mice with MASH. (**A**) Changes in body weight during the experiment. (**B**) The liver weight after treatment. (**C**) The ratio of liver weight to body weight after treatment. (**D**) The levels of serum ALT after treatment. (**E**) The levels of serum AST after treatment. (**F**) The levels of serum TC after treatment. (**G**) The levels of serum TG after treatment. (**H**) The levels of serum HDL-c after treatment. (**I**) The levels of serum LDL-c after treatment. (**J**) The levels of MDA after treatment. (**K**) The levels of SOD after treatment. (**L**) The levels of IL-6 after treatment. (**M**) The levels of TNF-α after treatment. (**N**) Oil-red-O staining was used to visualize lipid droplets in hepatocytes (×400). (**O**) H&E staining was used to visualize the pathological condition of the liver (×400). A-M: Data from ten independent replicates are presented as the mean ± SD. ** $P < 0.01$. (**N–O**): Data from three independent replicates are presented as the mean ± SD. ** $P < 0.01$.

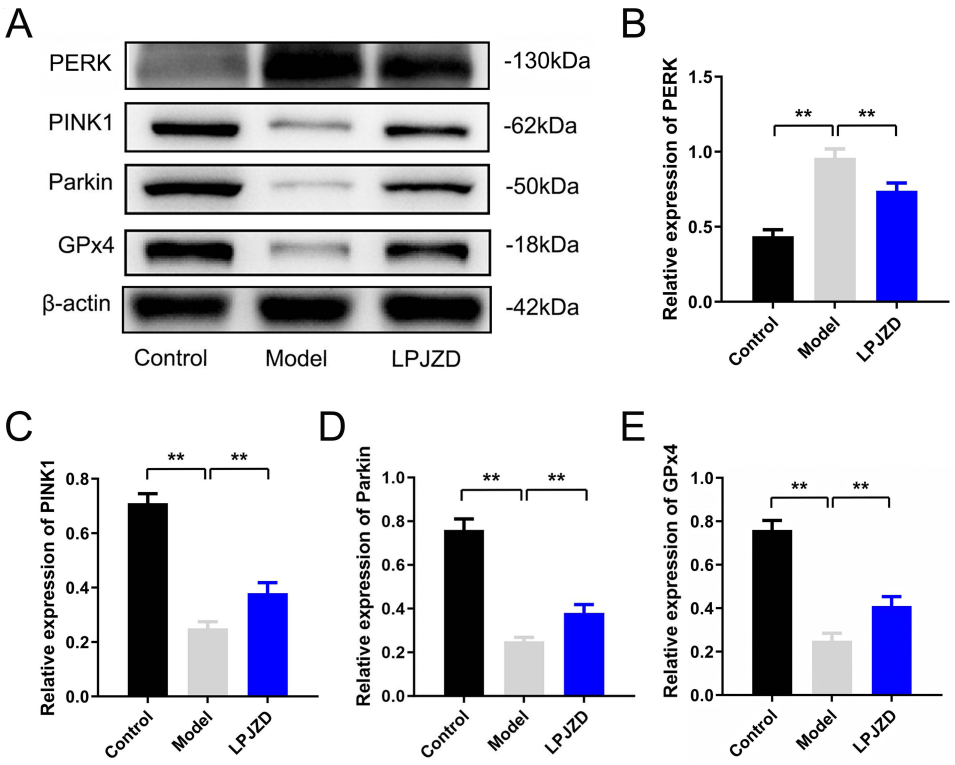

Figure 3 Effects of LPJZD on ER stress, mitophagy, and ferroptosis in the MASH mice. (**A**) Western blot analysis was performed to determine the protein expression levels of PERK, PINK1, Parkin, and GPx4. (**B**–**E**): Quantification of protein expression levels of PERK, PINK1, Parkin, and GPx4. Western blot quantification for each indicator was based on sampled from three mice, and the three mice were randomly selected from a corresponding experimental group. Data from three mice are presented as the mean ± SD. ** $P < 0.01$.

the protein expression levels of PINK1 and Parkin in the LPJZD group were significantly increased ($P<0.01$), indicating that key proteins involved in mitophagy were activated. In addition, we also detected changes in the level of glutathione peroxidase 4 (GPx4), which is closely related to ferroptosis (Figure 3A–E). The protein expression level of GPx4 in the model group was significantly lower than that in the control group ($P<0.01$). However, compared with the model group, the protein expression level of GPx4 in the LPJZD group was significantly increased ($P<0.01$), indicating that this key protein associated with ferroptosis was activated.

LPJZD Inhibits Ferroptosis by Enhancing the Expression of GPx4 in Liver Cells with MASH

The effects of LPJZD on ferroptosis in MASH liver cells were examined using immunofluorescence staining to assess the levels of Fe^{2+} and GPx4 in liver cells. The results revealed that, compared with the control group, the model group and RSL3 group had significantly increased Fe^{2+} content ($P<0.01$). Additionally, compared with the model group, the content of Fe^{2+} in the LPJZD group significantly decreased ($P<0.01$), and compared with the RSL3 group, the content of Fe^{2+} in the RSL3+LPJZD group also significantly decreased ($P<0.01$), indicating that LPJZD can effectively reduce the content of Fe^{2+} in MASH liver cells (Figure 4A and B). In addition, compared with the control group, the GPx4 levels in the model group and RSL3 group were significantly reduced ($P<0.01$). Moreover, compared with the model group, the level of GPx4 in the LPJZD group significantly increased ($P<0.01$), and compared with the RSL3 group, the level of GPx4 in the RSL3+LPJZD group also significantly increased ($P<0.01$), indicating that LPJZD can effectively increase the level of GPx4 in MASH liver cells (Figure 4C and D).

ROS levels in the liver cells were detected using a DCFH-DA fluorescent probe. The results showed that, compared with the control group, the ROS levels in the model group and RSL3 group were significantly increased ($P<0.01$). Also, compared with the model group, the level of ROS in the LPJZD group was significantly decreased ($P<0.01$), and

https://doi.org/10.2147/JIR.S532630

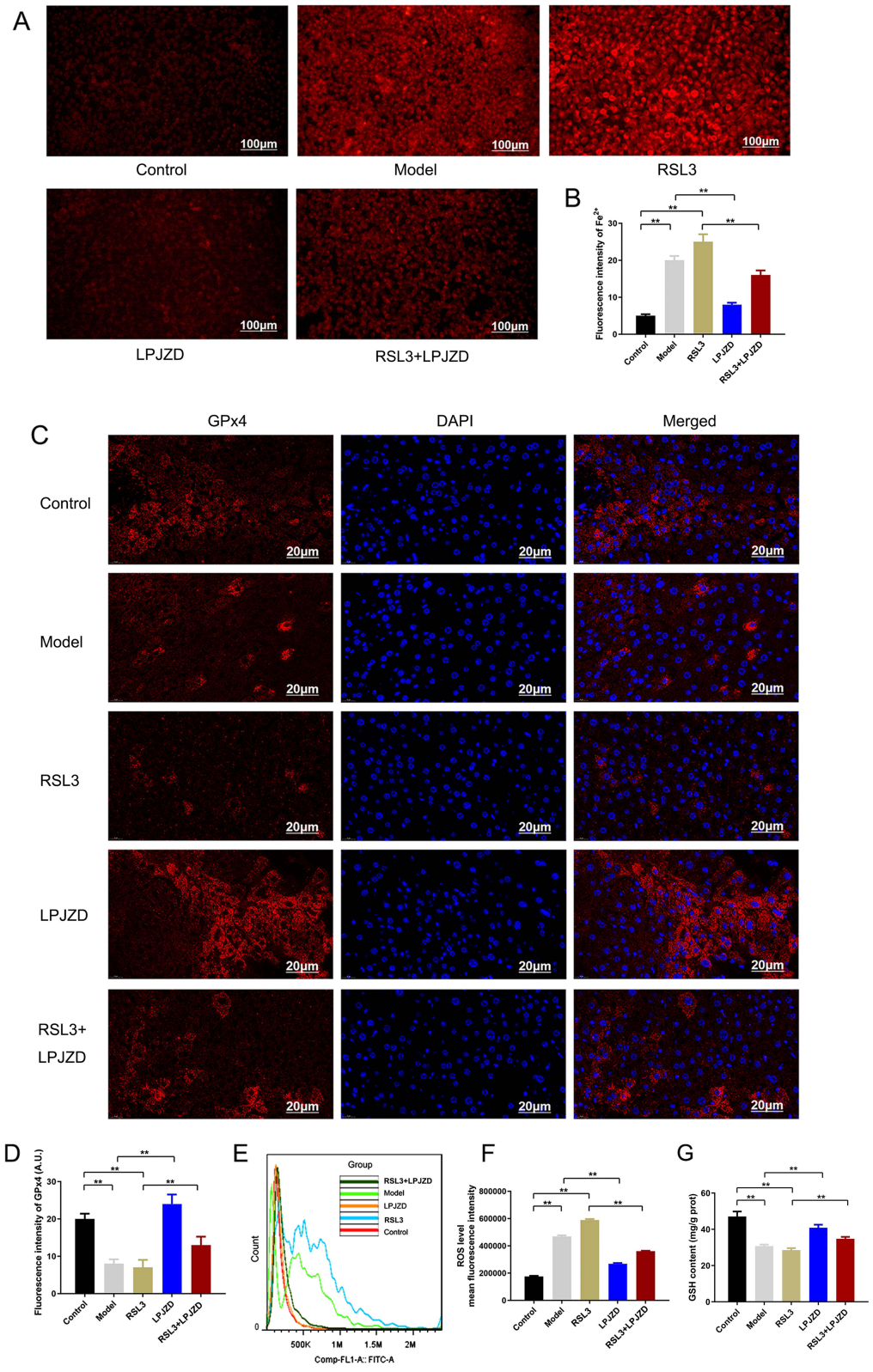

Figure 4 LPJZD inhibits ferroptosis in MASH liver cells. (**A**) The levels of Fe^{2+} were detected by immunofluorescence staining (×50). (**B**) Quantification of the Fe^{2+} levels. (**C**) The levels of GPx4 were detected by immunofluorescence staining (×100). (**D**) Quantification of the GPx4 levels. (**E**) The levels of ROS were detected by a flow cytometry method using the DCFH-DA fluorescent probe. (**F**) Quantification of ROS levels. (**G**) The levels of GSH. Data from three independent replicates are presented as the mean ± SD. ** $P < 0.01$.

compared with the RSL3 group, the ROS level in the RSL3+LPJZD group was also significantly decreased ($P<0.01$), indicating that LPJZD can effectively reduce the ROS level by enhancing the expression of GPx4 in MASH liver cells (Figure 4E and F). In addition, we also measured GSH content in liver cells using a GSH detection kit. The results showed that, compared with the control group, the GSH contents in the model group and RSL3 group were significantly decreased ($P<0.01$). Additionally, compared with the model group, the GSH content in LPJZD group significantly increased ($P<0.01$), and compared with the RSL3 group, the GSH content in the RSL3+LPJZD group was also significantly increased ($P<0.01$), indicating that LPJZD can effectively increase the GSH content by enhancing the expression of GPx4 in MASH liver cells (Figure 4G).

Morphological changes in mitochondria were observed by scanning electron microscopy, and the results showed that the liver cell matrix in model group and RSL3 group became thinner, the mitochondria swelled more into a circular shape, the membrane density increased, the mitochondrial cristae decreased, and the phenomenon of mitochondrial cristae reduction and rupture occurred, all of which indicated ferroptosis. After treatment, the liver cell mitochondria in the LPJZD group and RSL3+LPJZD group were mostly elongated without significant swelling, with an electron-dense matrix and clear mitochondrial cristae. These results suggest that LPJZD can inhibit ferroptosis by increasing the expression of GPx4 (Figure 5A).

Cell viability was assessed by MTT assay, which revealed that LPJZD at doses of 0.15 and 0.30 mg/mL had no effect on cell viability (Figure 5B). However, LPJZD at a dose of 0.15 mg/mL did not significantly reduce the inflammatory response (Figure 5C and D). Therefore, a dose of 0.30 mg/mL of LPJZD was subsequently used in the in vitro experiments. In addition, measurement of apoptosis by flow cytometry revealed that, compared with the control group, the model group and RSL3 group showed a significant increase in apoptosis ($P<0.01$). Additionally, compared with the model group, the LPJZD group showed a significant decrease in apoptosis ($P<0.01$), and compared with the RSL3 group, apoptosis in the RSL3+LPJZD group was significantly reduced ($P<0.01$), indicating that LPJZD can effectively reduce MASH liver cell apoptosis by increasing the expression of GPx4 (Figure 5E and F).

LPJZD Induces Mitophagy Through the PINK1/Parkin Signaling Pathway in MASH Liver Cells

This study assessed the effect of LPJZD on mitophagy and ferroptosis by examining whether it inhibits the mitophagy pathway PINK1/Parkin in liver cells. We found that, compared with the control group, the model group and mdivi-1 group showed decreased protein levels of PINK1 and Parkin ($P<0.01$), and compared with the model group, the protein levels of PINK1 and Parkin in LPJZD group were significantly increased ($P<0.01$). Additionally, compared with the mdivi-1 group, the protein level of PINK1 in the mdivi-1+LPJZD group was significantly increased ($P<0.01$), indicating that LPJZD can induce the PINK1/Parkin pathway in liver cells (Figure 6A–C). In addition, compared with the control group, the protein levels of GPx4 in the model group and mdivi-1 group decreased ($P<0.01$). Also, compared with the model group, the protein level of GPx4 in the LPJZD group was significantly increased ($P<0.01$), and compared with the mdivi-1 group, the protein level of GPx4 in the mdivi-1+LPJZD group was significantly increased ($P<0.01$), indicating that through inhibition of the PINK1/Parkin pathway, LPJZD can inhibit the expression of the key protein GPx4 in ferroptosis (6A, 6D).

The observation of the changes of mitochondrial autophagosomes in liver cells by transmission electron microscopy revealed that, compared with the model group, the mitophagosome number was significantly increased in the LPJZD group ($P<0.01$). In addition, compared with the mdivi-1 group, the mitophagosome number in the mdivi-1+LPJZD group was also significantly increased ($P<0.01$). Therefore, LPJZD can increase the mitophagosome number in liver cells (Figure 6E and F). Measurement of the mitochondrial membrane potential (MMP) by JC-1 staining was performed to evaluate the normal function of mitochondria, and the drop in mitochondrial membrane potential, which is a landmark event in the early stage of apoptosis. The results showed that compared with the control group, the mitochondrial membrane potentials of the model group and mdivi-1 group were significantly decreased ($P<0.01$). Also, compared with the model group, the LPJZD group showed a significantly reduced declining trend in mitochondrial membrane potential ($P<0.01$). Additionally, compared with the mdivi-1 group, the decrease in the mitochondrial membrane potential was

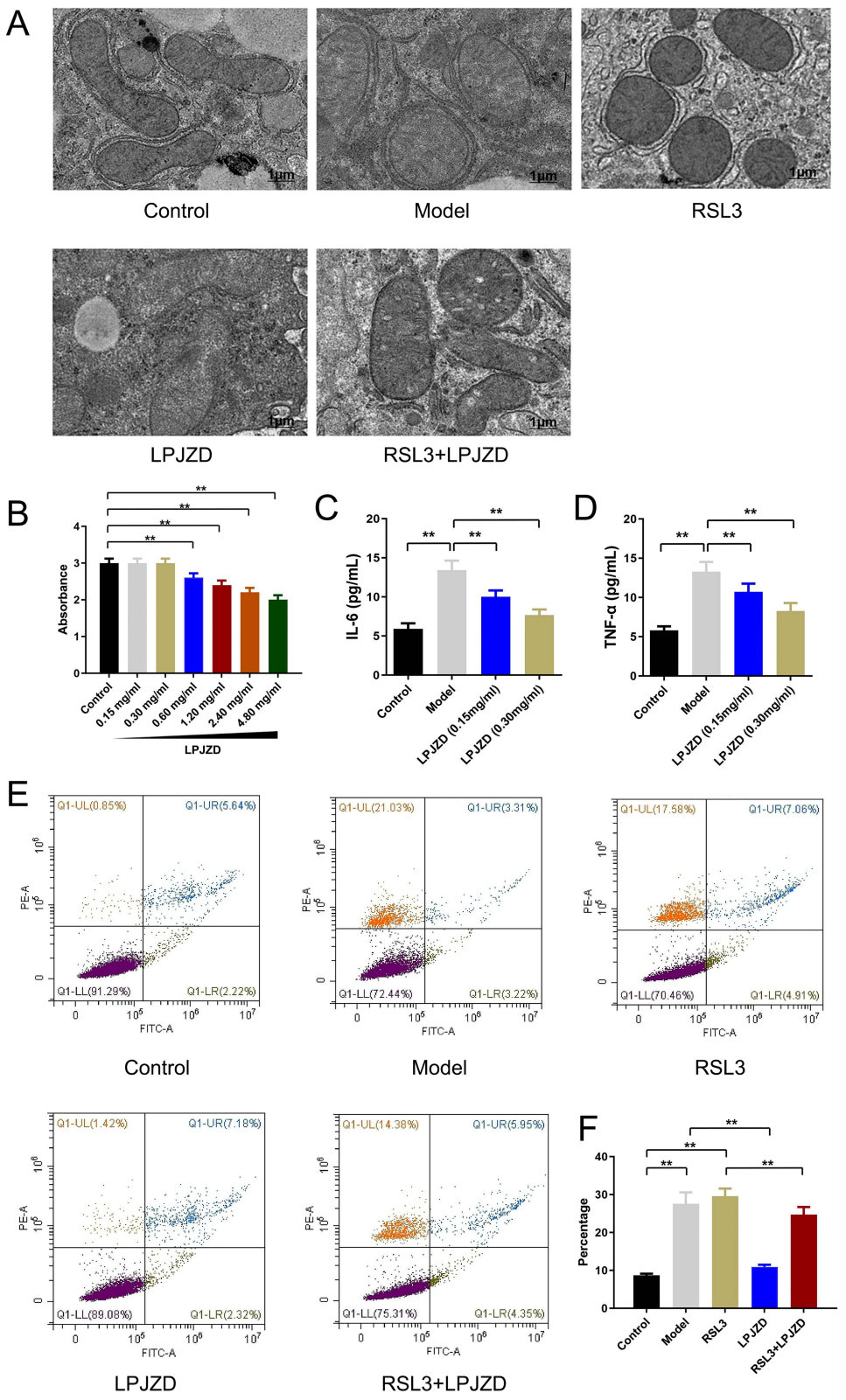

Figure 5 LPJZD inhibits ferroptosis, inflammatory response and apoptosis in MASH liver cells. (**A**) The morphological changes of mitochondria were observed by scanning electron microscopy (×20000). (**B**) Evaluation of the effect of different doses of LPJZD on cell viability using MTT assay. (**C** and **D**): Evaluation of the effect of different doses of LPJZD on the expression of IL-6 and TNF-α. (**E**) Evaluation of the effects of LPJZD on apoptosis using flow cytometry. (**F**) Quantification of apoptosis levels. Data from three independent replicates are presented as the mean ± SD. ** $P < 0.01$.

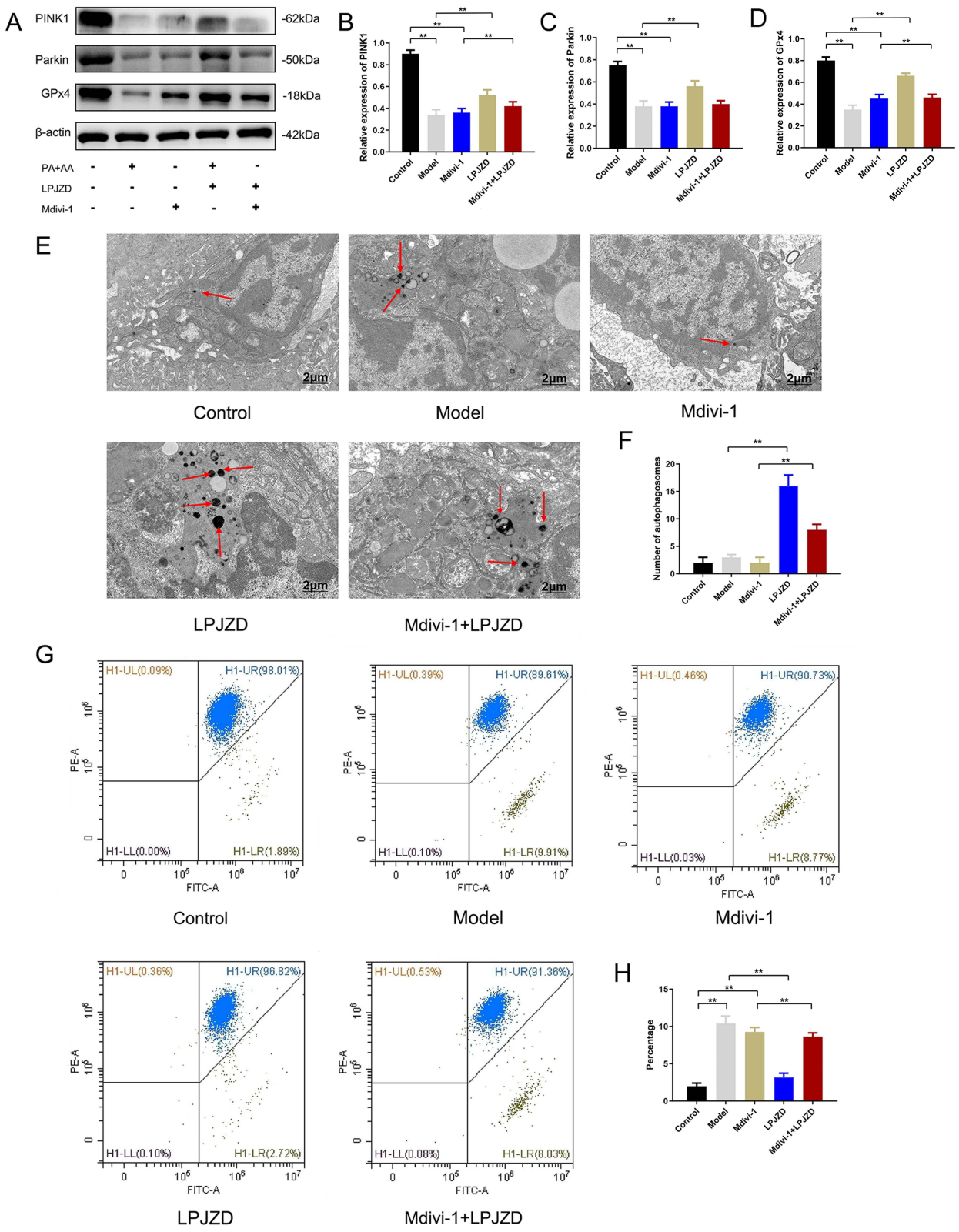

Figure 6 LPJZD induces mitophagy in MASH liver cells. (**A**) Western blot analysis was performed to determine the protein expression levels of PINK1, Parkin, and GPx4. (**B**–**D**): Quantification of protein expression levels of PINK1, Parkin, and GPx4. (**E**) Evaluation of the effect of LPJZD on mitochondrial autophagosomes using transmission electron microscopy (×10000). (**F**) Quantification of the mitophagosome number. (**G**) Evaluation of the effect of LPJZD on MMP. (**H**) Quantification of the effect of LPJZD on MMP. Data from three independent replicates are presented as the mean ± SD. ** $P < 0.01$.

https://doi.org/10.2147/JIR.S532630

reduced in the mdivi-1+LPJZD group (P<0.01), indicating that LPJZD can effectively inhibit the decrease in the mitochondrial membrane potential in MASH liver cells (Figure 6G and H).

This study also assessed whether LPJZD inhibits the PINK1/Parkin pathway in liver cells by examining the effects of LPJZD on Fe^{2+}, ROS, and GSH levels. The results showed that, compared with the control group, the Fe^{2+} levels in the model group and mdivi-1 group were significantly increased (P<0.01). Additionally, compared with the model group, the level of Fe^{2+} in the LPJZD group was significantly decreased (P<0.01), and compared with the mdivi-1 group, the level of Fe^{2+} in the mdivi-1+LPJZD group was also significantly decreased (P<0.01) (Figure 7A and B). Also, compared with the control group, the ROS levels in the model group and mdivi-1 group were significantly increased (P<0.01); compared with the model group, the level of ROS in the LPJZD group was significantly decreased (P<0.01); compared with the mdivi-1 group, the level of ROS in the mdivi-1+LPJZD group was also significantly decreased (P<0.01) (Figure 7C and D). In addition, compared with the control group, the GSH contents in the model group and mdivi-1 group were significantly reduced (P<0.01). Additionally, compared with the model group, the content of GSH in the LPJZD group was significantly increased (P<0.01), and compared with the mdivi-1 group, the content of GSH in the mdivi-1+LPJZD group was also significantly increased (P<0.01) (Figure 7E). These results indicate that, LPJZD can inhibit ferroptosis by activating PINK1/Parkin pathway.

In addition, measurement of apoptosis by flow cytometry showed that, compared with the control group, the model group and mdivi-1 group showed a significant increase in cell apoptosis (P<0.01). Additionally, compared with the model group, the LPJZD group showed a significant decrease in cell apoptosis (P<0.01), and compared with the mdivi-1 group, the mdivi-1+LPJZD group also showed a significantly decrease in cell apoptosis (P<0.01), indicating that LPJZD can effectively reduce apoptosis in MASH liver cells (Figure 7F and G).

LPJZD Inhibits ER Stress by Reducing PERK Expression in MASH Liver Cells

This study also evaluated the effects of LPJZD on mitophagy and ferroptosis following activation of PERK, the key protein in ER stress. The results showed that, compared with the control group, the protein expression levels of PERK increased in the model group and CCT group (P<0.01). Additionally, compared with the model group, the protein expression level of PERK in the LPJZD group was significantly decreased (P<0.01), and compared with the CCT group, the protein expression level of PERK in the CCT+LPJZD group was also significantly decreased (P<0.01) (Figure 8A and B). Western blot analysis of key proteins involved in mitophagy revealed that, compared with the control group, the protein expression levels of PINK1 and Parkin in the model group and CCT group were significantly decreased (P<0.01). Additionally, compared with the model group, the protein expression levels of PINK1 and Parkin in the LPJZD group significantly increased (P<0.01), and compared with the CCT group, the protein expression levels of PINK1 and Parkin in the CCT+LPJZD group were also significantly increased (P<0.01) (Figure 8A–D). Western blot analysis of a key protein involved in ferroptosis showed that, compared with the control group, the protein expression levels of GPx4 in the model group and CCT group were significantly decreased (P<0.01). Additionally, compared with the model group, the protein level of GPx4 in the LPJZD group was significantly increased (P<0.01), and compared with the CCT group, the protein level of GPx4 in the CCT+LPJZD group was also significantly increased (P<0.01) (Figure 8A–E). In addition, immunofluorescence staining analysis showed that, compared with the control group, the levels of glucose regulatory protein 78 (GRP78) in the model group and CCT group were significantly increased (P<0.01). Additionally, compared with the model group, the level of GRP78 in the LPJZD group was significantly decreased (P<0.01), and compared with the CCT group, the level of GRP78 in the CCT+LPJZD group was also significantly decreased (P<0.01) (Figure 8F and G). These results indicate that PERK activation reduces the expression levels of PINK1, Parkin, and GPx4, but LPJZD can reverse this trend.

The observation of the changes in the mitophagosome number in liver cells by transmission electron microscopy showed that, compared with the model group, the mitophagosome number was significantly increased in the LPJZD group (P<0.01). In addition, compared with the CCT group, the mitophagosome number in the CCT+LPJZD group was also significantly increased (P<0.01) (Figure 9A and B). The results of MMP measurements by JC-1 staining showed that, compared with the control group, the decrease in MMP was significantly increased in the model group and CCT group (P<0.01). Additionally, compared with the model group, the decrease in MMP in the LPJZD group was reduced (P<0.01), and compared with the CCT group, the decrease in MMP in the CCT+LPJZD group was also decreased

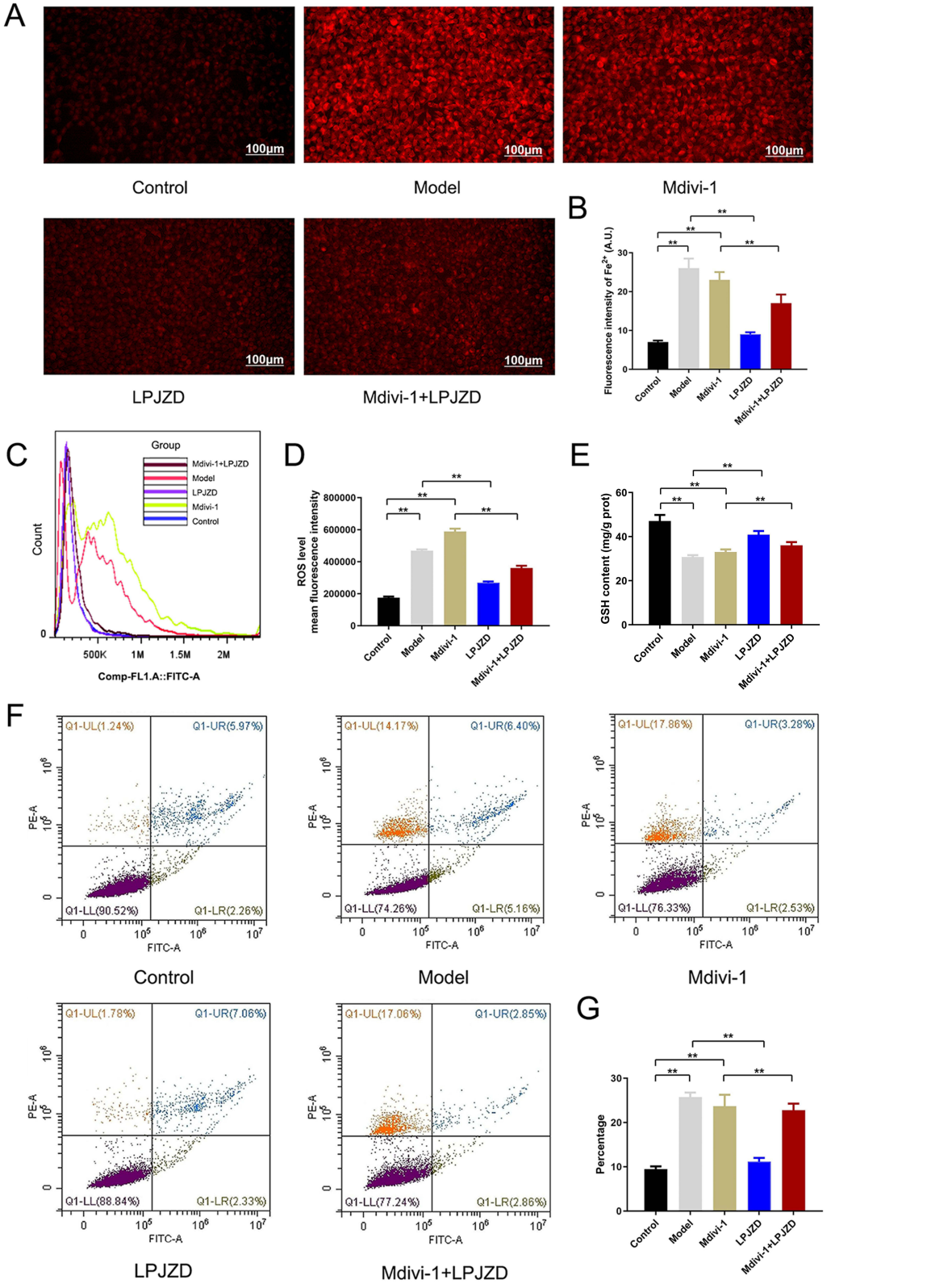

Figure 7 The effect of LPJZD on ferroptosis after inhibition of mitophagy in MASH liver cells. (**A**) The levels of Fe^{2+} was determined by immunofluorescence staining (×50). (**B**) Quantification of the Fe^{2+} levels. (**C**) The levels of ROS were determined by flow cytometry using the DCFH-DA fluorescent probe. (**D**) Quantification of the ROS levels. (**E**) The levels of GSH. (**F**) Evaluation of the effect of LPJZD on apoptosis by flow cytometry. (**G**) Quantification of apoptosis levels. Data from three independent replicates are presented as the mean ± SD. ** $P < 0.01$.

https://doi.org/10.2147/JIR.S532630

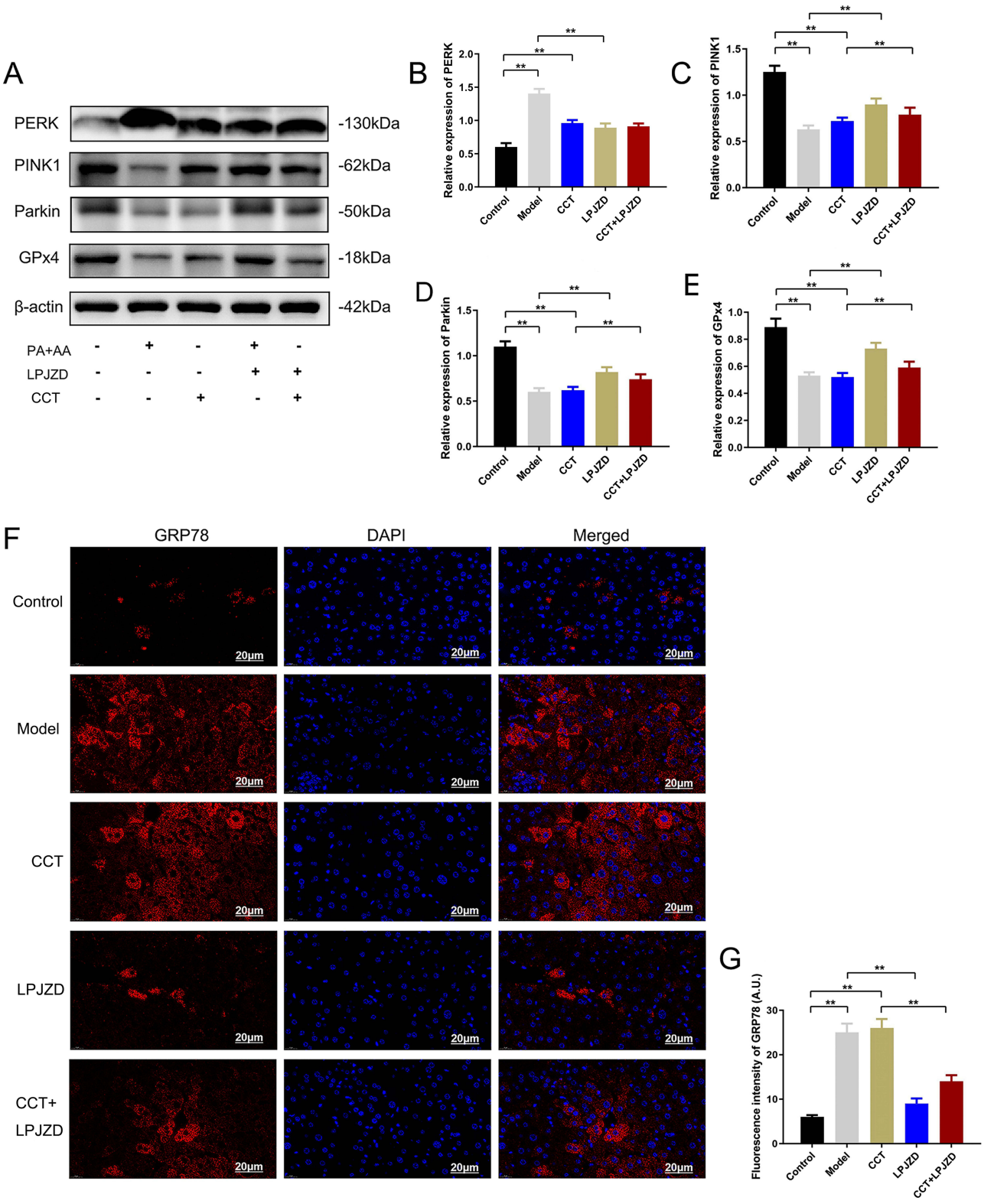

Figure 8 LPJZD inhibits ER stress in MASH liver cells. (**A**) Western blot analysis was performed to determine the protein expression levels of PERK, PINK1, Parkin, and GPx4. (**B**–**E**): Quantification of protein expression levels of PERK, PINK1, Parkin, and GPx4. (**F**) Evaluation of the effect of LPJZD on GRP78 protein expression using immunofluorescence staining (×100). (**G**) Quantification of GRP78 protein levels. Data from three independent replicates are presented as the mean ± SD. ** $P < 0.01$.

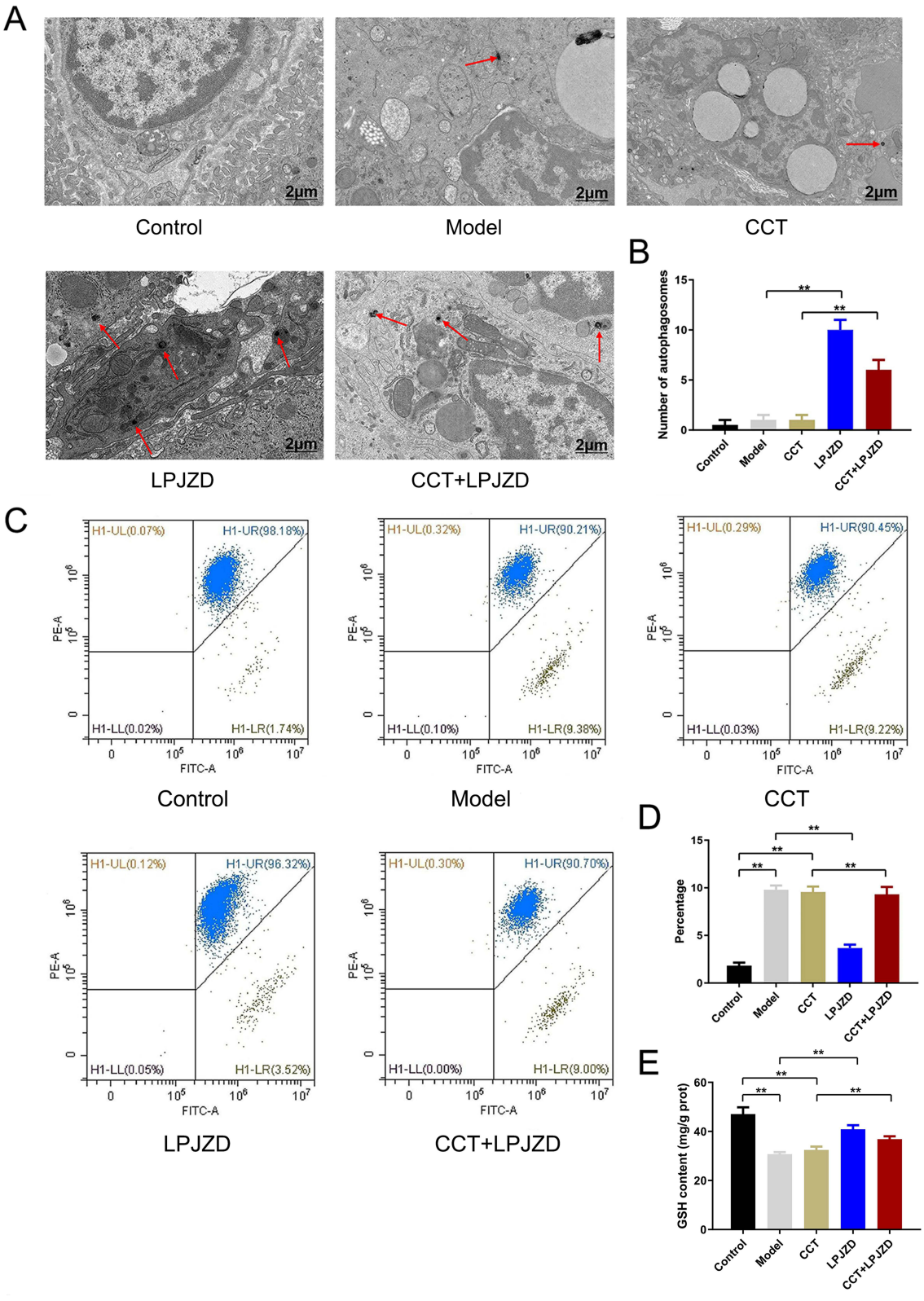

Figure 9 Continued.

https://doi.org/10.2147/JIR.S532630

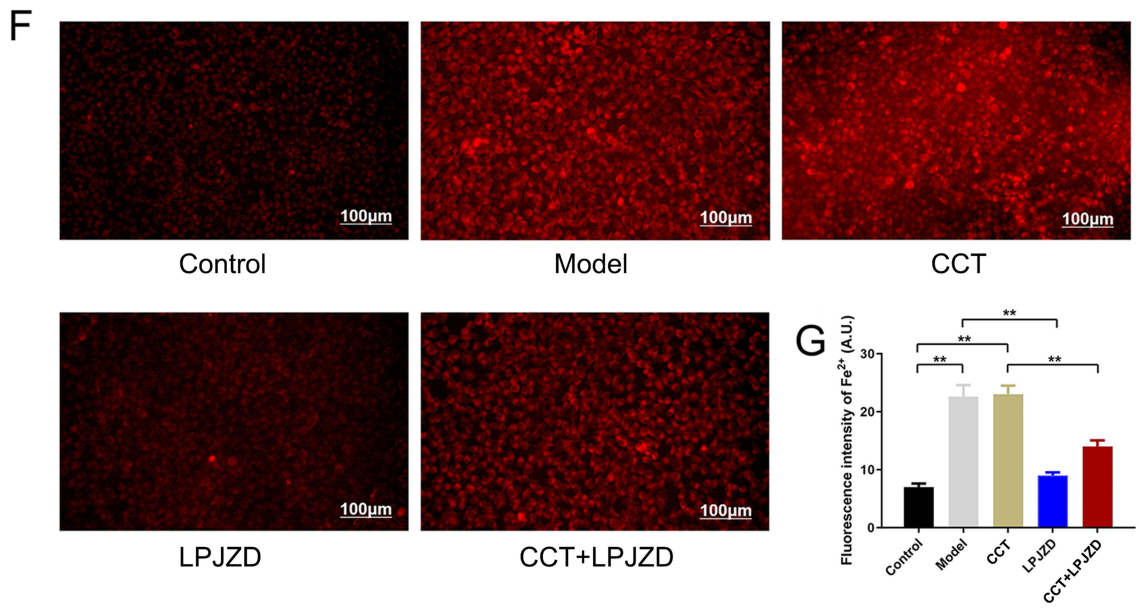

Figure 9 Effects of LPJZD on mitophagy and ferroptosis in the presence of activated PERK in MASH liver cells. (**A**) Evaluation of the effect of LPJZD on mitochondrial autophagosomes by transmission electron microscopy (×10000). (**B**) Quantification of the mitophagosome number. (**C**) Evaluation of the effect of LPJZD on MMP. (**D**) Quantification of the effect of LPJZD on MMP. (**E**) Evaluation of the effect of LPJZD on GSH level. (**F**) Evaluation of the effect of LPJZD on Fe^{2+} content by immunofluorescence staining (×50). (**G**) Quantification of Fe^{2+} levels. Data from three independent replicates are presented as the mean ± SD. ** $P < 0.01$.

(P<0.01) (Figure 9C and D). These results indicate that LPJZD treatment can activate mitophagy by reducing PERK expression.

This study also examined the effects of LPJZD on GSH and Fe^{2+} levels in the presence of activated PERK in liver cells. The results showed that, compared with the control group, the GSH contents in the model group and CCT group were significantly reduced (P<0.01). Additionally, compared with the model group, the content of GSH in the LPJZD group was significantly increased (P<0.01), and compared with the CCT group, the content of GSH in the TM+LPJZD group was also significantly increased (P<0.01) (Figure 9E). For Fe^{2+}, compared with the control group, the Fe^{2+} contents in the model group and CCT group were significantly increased (P<0.01). In addition, compared with the model group, the content of Fe^{2+} in the LPJZD group was significantly decreased (P<0.01), and compared with the CCT group, the content of Fe^{2+} in the CCT+LPJZD group was also significantly decreased (P<0.01) (Figure 9F and G). These results indicate that treatment with LPJZD can reduce the expression of PERK, activate mitophagy, and inhibit ferroptosis in liver cells.

Discussion

MASH is closely associated with obesity, insulin resistance, dyslipidemia, lipotoxicity, oxidative stress, mitochondrial dysfunction, endocrine dysfunction, and metabolic syndrome. Its main characteristics include bullous hepatocyte steatosis, accompanied by hepatocyte injury and inflammation. To date, there are no effective treatments that can completely reverse MASH symptoms. Although weight loss or the use of drugs, such as reduced glutathione, silymarin, polyene phosphatidylcholine, vitamin E, and ursodeoxycholic acid, can alleviate the pathological symptoms of MASH, it is difficult to achieve a complete cure.[32] MASH belongs to the following disease categories in TCM: “fat qi”, “phlegm turbidity”, and “accumulation”. TCM believes that fat come from the essence of water and grains, and its generation and distribution depend on the transportation function of the spleen.[33] Under the guidance of syndrome differentiation and treatment, TCM formulas have the characteristics of multiple compounds, targets, and effects, and have shown unique advantages and good prospects in the prevention and treatment of MASH. Professor Zhou Ciqing, a nationally renowned expert in TCM, proposed a strategy of “regulating the spleen and reducing turbidity” to treat MASH. In clinical practice, the focus is on strengthening the spleen to play the role of “spleen governing circulation and transformation”, thereby

reducing the discharge of turbid yin. He created the LPJZD formula and obtained a national invention patent (patent number ZL00410024300x). Clinical applications have shown that LPJZD can significantly improve lipid metabolism disorders in MAFLD patients, and has no side effects.[15] This study found that LPJZD can reduce the accumulation of lipid droplets in the liver of MASH mice, liver tissue oxidation and liver cell inflammation, as well as enhance liver cell vitality. Therefore, in-depth exploration of the role and mechanism of LPJZD can provide an important theoretical basis for its widespread clinical application.

Moreover, multiple studies have confirmed that the active compounds in LPJZD can improve MASH. Data from Q-Orbitrap high-resolution LC-MS analysis revealed 35 compounds with best match scores greater than 90, including formononetin, berberine, quercetin, genistein, rutin, daidzein, and naringin, etc. Some studies have indicated that many of these compounds have lipid-lowering and anti-inflammatory effects. Previous studies have shown that formononetin treatment can promote fatty acid β oxidation and regulate liver lipid metabolism, ultimately improving MASH liver cell steatosis.[34] Berberine has anti-inflammatory, anti-obesity, and hepatoprotective properties, and is an effective drug for the treatment of MASH. Farnesol X receptor (FXR) is a bile acid receptor and a drug target for the treatment of MASH. Additionally, berberine can alleviate MASH by regulating the interaction between gut microbiota and bile acid metabolism, as well as the subsequent activation of intestinal FXR.[35] Quercetin is a flavonoid compound that exhibits strong antioxidant properties and significantly reduces lipid accumulation in steatotic cells. Studies indicate that quercetin markedly reduces production of IL1B, IL-6, and TNF-α, and ameliorates MAFLD by promoting AMPK-mediated liver mitophagy.[20] Genistein treatment can reduce fat accumulation in the liver and ameliorate MASH through the upregulation of PPARα, and PPARδ, and the suppression of PPARγ and STAT1 expression.[36] Rutin can reduce body weight and fat mass in obese mice, alleviates liver inflammation, and demonstrates promising therapeutic potential by restricting the progression of liver injury and modulating dysregulated lipid metabolism.[37] The study found that MAFLD prevalence, controlled attenuation parameter, hepatic steatosis index, and fatty liver index, all decreased with increased daidzein intake, suggesting that daidzein intake may improve hepatic steatosis.[38] Naringin can reduce liver lipid accumulation in MAFLD rats, and downregulate the NLRP3/NF-κB pathway to reduce liver inflammation.[39] Therefore, a variety of active compounds of LPJZD can effectively treat MASH.

The endoplasmic reticulum is an important site for protein synthesis and folding in eukaryotic organisms, and is an essential organelle for maintaining normal life activities. Exogenous substances, oxidative stress, hypoxia, and the accumulation of non-folding proteins in the endoplasmic reticulum can all alter the balance of the endoplasmic reticulum, leading to ER stress and disrupting its integrity.[40] Studies have shown that ER stress plays an important role in the pathogenesis of MASH. Garcia-Carbonero et al, found that the specific deficiency of BIP/GRP78 in mouse liver can cause ER stress, ultimately leading to hepatic steatosis and hepatocyte apoptosis.[41] In addition, there is an imbalance in ER homeostasis in the liver and adipose tissue of patients with MASH. In the MASH model established by Li et al, the expression of inflammatory factors and ER stress-related apoptotic proteins in the liver was increased.[42] These results suggest that ER stress in MASH is inevitably associated with the occurrence of the inflammatory response and apoptosis. PERK is a major mediator of ER stress and a marker of ER stress initiation. It is involved in regulating basic cellular functions, and ER stress-induced apoptosis and autophagy signals can be transduced through the PERK pathway to trigger cell death.[43] GRP78 plays a critical role in protein folding, processing, proteasome-mediated cell lysis, attacking and targeting misfolded proteins, and other cellular activities. It is an important biomarker of the ER stress response.[44] The results of this study indicate that LPJZD can reduce the expression of the ER stress marker proteins PERK and GRP78 in MASH liver cells, effectively inhibiting ER stress.

ER stress is one of the main causes of mitochondrial dysfunction, and the endoplasmic reticulum and mitochondrial dialogue have been shown to play important roles in the pathogenesis of MASH.[45] Mitophagy can degrade damaged mitochondria and misfolded proteins in the liver to regulate cell death, while maintaining dynamic lipid balance within liver cells. In addition, it is a key pathway for maintaining lipid metabolism homeostasis.[46] Research has shown that when lipid accumulation in the liver increases, it causes a decrease in mitophagy levels, inhibits the binding of autophagosomes to lysosomes, and affects the role of autophagy in lipid degradation. If the autophagy level of liver mitochondria is restored, it can then degrade lipid droplets in liver cells and release free fatty acids into intracellular mitochondria where fatty acid β- oxidation regulates lipid storage and energy balance within liver cells, thereby

preventing the occurrence of MASH.[47,48] The Pink1/Parkin signaling pathway-mediated mitophagy is a classic regulatory mechanism. In normal cells, proteolytic enzyme-hydrolyzed PINK1 shows low expression levels. When mitochondrial function is impaired, it causes a drop or disappearance of the MMP, and mitochondria cannot degrade PINK1 in a timely manner, leading to excessive accumulation in the outer mitochondrial membrane and inducing mitophagy.[49] Yao et al found that PINK1/Parkin can protect liver cells and participate in MASH by clearing damaged mitochondria.[11] The results of this study indicate that LPJZD can increase the expression of the mitophagy proteins PINK1 and Parkin in MASH liver cells, increase the mitophagosome number, restore MMP, and effectively improve MASH by enhancing mitophagy.

Ferroptosis is an iron ion-dependent and non-apoptotic form of cell death characterized by the accumulation of intracellular lipid and ROS. Chen et al pointed out that ferroptosis is the earliest form of cell death in MASH, and specific inhibition of ferroptosis can almost completely inhibit liver tissue inflammation.[12] Studies have shown that approximately one-third of MAFLD patients exhibit signs of iron homeostasis dysregulation, mainly manifested as elevated serum ferritin. Pierantonelli et al reported that serum ferritin levels in MAFLD patients were greater than 1.5 times the upper limit of the normal value, which is closely related to liver iron deposition and histological inflammation.[50] Therefore, an increase in serum ferritin levels is an independent risk factor for the progression of MAFLD to MASH and fibrosis. Furthermore, clinical testing results of MASH patients show that serum ferritin and liver iron overload are common, and iron overload is an important biochemical feature of ferroptosis. Tsuchida et al confirmed the occurrence of ferroptosis in a diet-induced MASH mouse model with methionine choline deficiency. Furthermore, ferroptosis inhibitors can completely reduce lipid droplets in liver cells, improve liver histology, reduce oxidative stress, normalize lipogenesis, protect liver cells from death, and inhibit inflammatory response, suggesting that ferroptosis is the key to the pathogenesis and treatment of MASH.[51]

In addition, ferroptosis is mainly caused by the excessive accumulation of iron ion-induced ROS in cells, which reduces the clearance effect of GPx4 and disrupts the homeostatic balance of ROS generation and degradation.[52] A study has shown that PINK1/Parkin-mediated mitophagy can inhibit ferroptosis via two pathways.[8] First, excessive Fe^{2+} and hydrogen peroxide-induced iron-dependent Fenton reaction can increase ROS and phospholipid hydroperoxide (PLOOH) levels, further promoting ferroptosis. PINK1/Parkin-mediated mitophagy can inhibit the production of excessive Fe^{2+}, thereby blocking the Fenton reaction and inhibiting ferroptosis. Second, the activation of the PINK1/Parkin pathway can lead to the reduction of excessive ROS release, thereby decreasing the downregulation of GPx4. The enzyme GPx4 directly catalyzes the conversion of endogenous PLOOH into harmless lipid alcohols using GSH as a substrate, thus reducing lipid peroxidation levels and inhibiting ferroptosis (Figure 10). Currently, GPx4 has become an important reference marker to determine lipid peroxidation. Knockout of GPx4 can cause a significant increase in lipid peroxidation

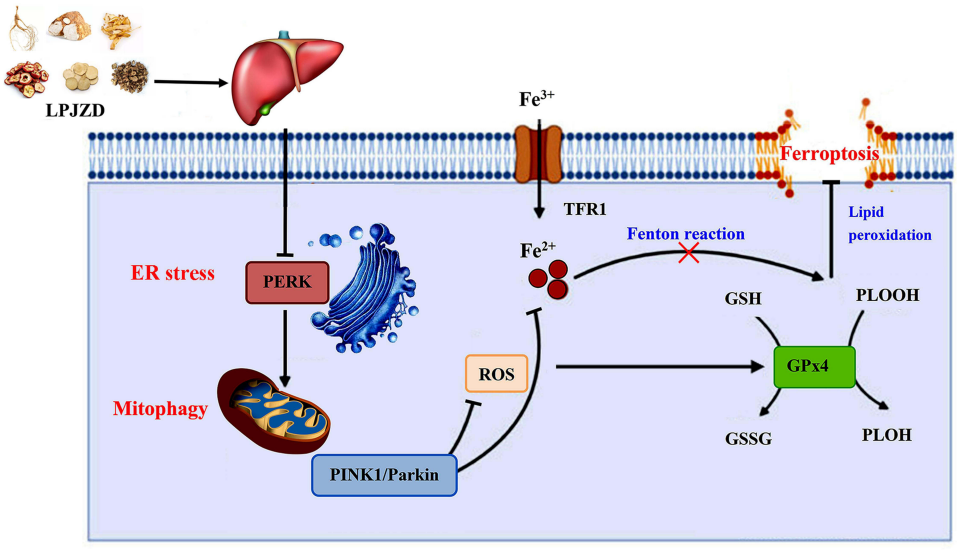

Figure 10 Schematic representation of the mechanism of action of LPJZD in alleviating MASH.

levels, which can induce ferroptosis.[47] Ferroptosis can participate in the inflammatory response process, thereby inducing MASH. The results of this study indicate that LPJZD can improve mitochondrial swelling in MASH liver cells, reduce Fe^{2+} and ROS levels in liver cells, enhance GPx4 protein expression and GSH content, and effectively reduce apoptosis. Therefore, LPJZD may activate mitophagy by acting on the PINK1/Parkin pathway, thereby inhibiting ferroptosis in liver cells and contributing to the prevention and treatment of MASH.

In brief, this study possesses some advantages. Firstly, this study reveals that LPJZD can ameliorate MASH by regulating the PERK/PINK1/GPx4 pathway, proposing a multi-target mechanism simultaneously targeting ER stress, mitophagy, and ferroptosis. This discovery complements the current single-target strategies of mainstream drugs and provides a novel approach for developing comprehensive therapies. Secondly, currently approved drugs resmetirom and semaglutide face gastrointestinal adverse effects or cardiovascular safety concerns.[53,54] The natural components of LPJZD may reduce the risk of side effects, particularly suiting the need for long-term medication, so LPJZD can offer superior safety advantages. However, although this study reveals the role of LPJZD in ameliorating MASH through regulation of the PERK/PINK1/GPx4 pathway, there are still potential limitations in the research mechanism. For instance, the upstream/downstream regulatory mechanisms of this pathway remain unclear. Therefore, we can further utilize drug affinity responsive target stability technology combined with LC-MS to explore targets of LPJZD along the PERK/PINK1/GPx4 pathway in hepatocytes, aiming to identify key factors through which LPJZD modulates this pathway.

Conclusion

This study focuses on the novel pharmacological mechanism of the treatment of MASH with LPJZD, and proposes that in the treatment of MASH, LPJZD can inhibit hepatic PERK and ER stress, activate mitophagy by regulating the PINK1/Parkin signaling pathway, inhibit Fe^{2+} formation, reduce lipid ROS accumulation, relieve the decline of GPx4 levels, reduce lipid peroxidation levels, inhibit liver cell ferroptosis, and thus play a role in improving the inflammatory response in MASH. The significance of this study is in providing a new scientific explanation of the mechanism of treating MASH with the formula for regulating spleen and reducing turbidity, and providing research ideas and methods for treating MASH by targeting ER stress, mitophagy, and ferroptosis.

Abbreviations

AA, arachidonic acid; ALT, alanine aminotransferase; AST, aspartate aminotransferase; CCT, CCT020312; ER, endoplasmic reticulum; ESI, electrospray ionization; Fe^{2+}, ferrous ion; GRP78, glucose regulatory protein 78; GSH, intracellular glutathione; HDL-c, high-density lipoprotein cholesterol; H&E, hematoxylin and eosin; IL-6, interleukin 6; LC-MS, liquid chromatography and mass spectrometry; LDL-c, low-density lipoprotein cholesterol; LPJZD, Lipi Jiangzhuo decoction; MDA, malondialdehyde; MTT, methyl thiazole tetrazolium; MAFLD, metabolic dysfunction-associated fatty liver disease; MASH, metabolic dysfunction-associated steatohepatitis; OD, optical density; PA, palmitic acid; PBS, phosphate-buffered saline; PERK, protein kinase R-like endoplasmic reticulum kinase; SD, standard deviation; SOD, superoxide dismutase; TBST, Tris-buffered saline with 0.1% Tween 20; TC, total cholesterol; TCM, traditional Chinese medicine; TG, triglyceride; TNF-α, tumor necrosis factor-alpha.

Data Sharing Statement

The datasets analyzed during the current study are available from the corresponding author on reasonable request.

Ethical Statement

This study was approved by the Animal Ethics Committee of Shandong University of Traditional Chinese Medicine with the permit number: SDUTCM20220707005.

Author Contributions

All authors made significant contributions to the work, whether in the conception, study design, execution, data acquisition, analysis, interpretation, or all these areas. They took part in drafting, revising, or critically reviewing the

article; gave final approval to the published version; agreed to submit the article to this journal; and agreed to be accountable for all aspects of the work.

Funding

This study was supported by the Shandong Provincial Natural Science Foundation Project (ZR2023QH101); Shandong Province Medical and Health Technology Project (202403060392); Inheritance Project of TCM Academic Schools of Qilu Medical School: Qilu Zhiyuan Academic School Inheritance Project (No.[2022]93).

Disclosure

The authors declare that the research was conducted in the absence of any commercial or financial relationships that could be construed as a potential conflict of interest.

References

1. Sanyal AJ, Van Natta ML, Clark J, et al. Prospective study of outcomes in adults with nonalcoholic fatty liver disease. *N Engl J Med*. 2021;385(17):1559–1569. doi:10.1056/NEJMoa2029349
2. Powell EE, Wong VW, Rinella M. Non-alcoholic fatty liver disease. *Lancet*. 2021;397(10290):2212–2224. doi:10.1016/S0140-6736(20)32511-3
3. Zhou F, Zhou J, Wang W, et al. Unexpected rapid increase in the burden of NAFLD in China from 2008 to 2018: a systematic review and meta-analysis. *Hepatology*. 2019;70(4):1119–1133. doi:10.1002/hep.30702
4. Francque S, Szabo G, Abdelmalek MF, et al. Nonalcoholic steatohepatitis: the role of peroxisomeproliferator-activated receptors. *Nat Rev Gastroenterol Hepatol*. 2021;18(1):24–39. doi:10.1038/s41575-020-00366-5
5. Younossi ZM, Golabi P, Price JK, et al. The global epidemiology of nonalcoholic fatty liver disease and nonalcoholic steatohepatitis among patients with type 2 diabetes. *Clin Gastroenterol Hepatol*. 2024;22(10):1999–2010.e8. doi:10.1016/j.cgh.2024.03.006
6. Targher G, Byrne CD, Tilg H. MASLD: a systemic metabolic disorder with cardiovascular and malignant complications. *Gut*. 2024;73(4):691–702. doi:10.1136/gutjnl-2023-330595
7. Keam SJ. Resmetirom: first approval. *Drugs*. 2024;84(6):729–735. doi:10.1007/s40265-024-02045-0
8. Shakeel L, Shaukat A, Akilimali A. Resmetirom: a breakthrough in the treatment of metabolic dysfunction-associated steatotic liver disease (MASLD). *Health Sci Rep*. 2025;8(6):e70920. doi:10.1002/hsr2.70920
9. Chen Z, Tian R, She Z, et al. Role of oxidative stress in the pathogenesis of nonalcoholic fatty liver disease. *Free Radic Biol Med*. 2020;152:116–141. doi:10.1016/j.freeradbiomed.2020.02.025
10. Almeida LM, Pinho BR, Duchen MR, et al. The PERKs of mitochondria protection during stress: insights for PERK modulation in neurodegenerative and metabolic diseases. *Biolog Rev Cambridge Philosophical Soc*. 2022;97(5):1737–1748. doi:10.1111/brv.12860
11. Yao Z, Li X, Wang W, et al. Corn peptides attenuate non-alcoholic fatty liver disease via PINK1/Parkin-mediated mitochondrial autophagy. *Food Nutrit Res*. 2023;67:10.29219/fnr.v67.9547. doi:10.29219/fnr.v67.9547
12. Chen J, Li X, Ge C, et al. The multifaceted role of ferroptosis in liver disease. *Cell Death Differ*. 2022;29(3):467–480. doi:10.1038/s41418-022-00941-0
13. Lin Q, Li S, Jin H, et al. Mitophagy alleviates cisplatin-induced renal tubular epithelial cell ferroptosis through ROS/HO-1/GPX4 axis. *Int J Bio Sci*. 2023;19(4):1192–1210. doi:10.7150/ijbs.80775
14. Pan LL, Xiang HJ, Liu GR. Exploring the mechanism of Lipi Jiangzhuo formula in improving nonalcoholic fatty liver disease in rats by regulating the HIF-1α/PPARγ/BNIP3 mitochondrial autophagy pathway. *Lishizhen Med Materia Medica Res*. 2024;35(8):1862–1867. doi:10.3969/j.issn.1008-0805.2024.08.16
15. Liu GR, Zhou CQ, Zou Y. Clinical Study of the Lipi Tiaozhi Capsule in the treatment of simple dyslipidemia. *J Shandong Univ Trad Chin Med*. 2002;3:179–181. doi:10.16294/j.cnki.1007-659x.2002.03.009
16. Yan S, Liu GR, Liu F. Effect of the Lipi Tiaozhi capsule on ApoE and ApoC gene expression in rats with dyslipidemia. *Shanghai J Traditional Chin Med*. 2011;45:60–62. doi:10.16305/j.1007-1334.2011.02.024
17. Pan LL, Sun QH, Liu JH, et al. Discussing the mechanism of Lipi Tiaozhi capsule on improving lipid metabolism disorder in hyperlipidemic rats based on metabonomics. *J Sichuan Trad Chin Med*. 2019;37(11):44–49.
18. Feng L, Riaz F, Lu K, et al. Leucine aminopeptidase 3:a promising serum biomarker candidate for nonalcoholic steatohepatitis diagnosis. *Int Immunopharmacol*. 2023;119:110152. doi:10.1016/j.intimp.2023.110152
19. Gart E, van Duyvenvoorde W, Caspers MPM, et al. Intervention with isoleucine or valine corrects hyperinsulinemia and reduces intrahepatic diacylglycerols, liver steatosis, and inflammation in Ldlr-/-.Leiden mice with manifest obesity-associated NASH. *FASEB j*. 2022;36(8):e22435. doi:10.1096/fj.202200111R
20. Cao P, Wang Y, Zhang C, et al. Quercetin ameliorates nonalcoholic fatty liver disease via the promotion of AMPK-mediated hepatic mitophagy. *J Nutr Biochem*. 2023;120:109414. doi:10.1016/j.jnutbio.2023.109414
21. Li D, Jiang C, Mei G, et al. Quercetin alleviates ferroptosis of pancreatic β cells in type 2 diabetes. *Nutrients*. 2020;12(10):2954. doi:10.3390/nu12102954
22. Um JH, Lee KM, Kim YY, et al. Berberine induces mitophagy through adenosine monophosphate-activated protein kinase and ameliorates mitochondrial dysfunction in PINK1 knockout mouse embryonic fibroblasts. *Int J Mol Sci*. 2023;25(1):219. doi:10.3390/ijms25010219
23. Yang KT, Chao TH, Wang IC, et al. Berberine protects cardiac cells against ferroptosis. *Tzu Chi Med J*. 2022;34(3):310–317. doi:10.4103/tcmj.tcmj_236_21
24. Yang W, Liu R, Sun Q, et al. Quercetin alleviates endoplasmic reticulum stress-induced apoptosis in buffalo ovarian granulosa cells. *Animals*. 2022;12(6):787. doi:10.3390/ani12060787

25. Liu QZ, Han H, Fang XR, et al. Berberine alleviates ovarian tissue damage in mice with hepatolenticular degeneration by suppressing ferroptosis and endoplasmic reticulum stress. *J Integr Med*. 2024;22(4):493–502. doi:10.1016/j.joim.2024.05.003
26. Hagiwara D, Azuma Y, Kawaguchi Y, et al. Response to endoplasmic reticulum stress in arginine vasopressin neurons. *Endocr J*. 2023;70(6):567–572. doi:10.1507/endocrj.EJ23-0193
27. Deng C, Yi R, Fei M, et al. Naringenin attenuates endoplasmic reticulum stress, reduces apoptosis, and improves functional recovery in experimental traumatic brain injury. *Brain Res*. 2021;1769:147591. doi:10.1016/j.brainres.2021.147591
28. Guo X, Guo Y, Li J, et al. Arginine expedites erastin-induced ferroptosis through fumarate. *Int J Mol Sci*. 2023;24(19):14595. doi:10.3390/ijms241914595
29. Xu S, Wu B, Zhong B, et al. Naringenin alleviates myocardial ischemia/reperfusion injury by regulating the nuclear factor-erythroid factor 2-related factor 2 (Nrf2) /System xc-/ glutathione peroxidase 4 (GPX4) axis to inhibit ferroptosis. *Bioengineered*. 2021;12(2):10924–10934. doi:10.1080/21655979.2021.1995994
30. Mouries J, Brescia P, Silvestri A, et al. Microbiota-driven gut vascular barrier disruption is a prerequisite for non-alcoholic steatohepatitis development. *J Hepatol*. 2019;71(6):1216–1228. doi:10.1016/j.jhep.2019.08.005
31. Nie YS, Yan M, Xie H, et al. Preparing method of obese rat model with spleen deficiency and phlegm dampness. *J Shanxi Univ Chin Med*. 2019;42(03):68–72. doi:10.13424/j.cnki.jsctcm.2019.03.019
32. Stefan N. New pharmacological treatment options for nonalcoholic fatty liver disease. *Der Internist*. 2020;61(7):759–765. doi:10.1007/s00108-020-00801-4
33. Zhang X, Hu ZB, Xu K, et al. Research progress of prevention and treatment of nonalcoholic fatty liver disease with TCM. *Henan Tradl Chin Med*. 2021;41(09):1427–1431. doi:10.16367/j.issn.1003-5028.2021.09.0323
34. Liao J, Xie X, Wang N, et al. Formononetin promotes fatty acid β-oxidation to treat non-alcoholic steatohepatitis through SIRT1/PGC-1α/PPARα pathway. *Phytomedicine*. 2024;124:155285. doi:10.1016/j.phymed.2023.155285
35. Shu X, Li M, Cao Y, et al. Berberine alleviates non-alcoholic steatohepatitis through modulating gut microbiota mediated intestinal FXR activation. *Front Pharmacol*. 2021;12:750826. doi:10.3389/fphar.2021.750826
36. Okrit F, Chayanupatkul M, Siriviriyakul P, et al. Genistein and sex hormone supplementation modulated hepatic PPARα, δ, and γ subtypes and STAT1 expressions in a NASH rat model with bilateral orchidectomy. *Biomedicines*. 2024;12(3):483. doi:10.3390/biomedicines12030483
37. Melini S, Pirozzi C, Lama A, et al. Co-micronized palmitoylethanolamide and rutin associated with hydroxytyrosol recover diabesity-induced hepatic dysfunction in mice: in vitro insights into the synergistic effect. *Phytother Res*. 2024;38(12):6035–6047. doi:10.1002/ptr.8361
38. Yang Z, Gong D, He X, et al. Association between daidzein intake and metabolic associated fatty liver disease: a cross-sectional study from NHANES 2017-2018. *Front Nutr*. 2023;10:1113789. doi:10.3389/fnut.2023.1113789
39. Wang Q, Ou Y, Hu G, et al. Naringenin attenuates non-alcoholic fatty liver disease by down-regulating the NLRP3/NF-κB pathway in mice. *B. Pharmacol*. 2020;177(8):1806–1821. doi:10.1111/bph.14938
40. Chen X, Shi C, He M, et al. Endoplasmic reticulum stress: molecular mechanism and therapeutic targets. *Signal Transduct Target Ther*. 2023;8(1):352. doi:10.1038/s41392-023-01570-w
41. Garcia-Carbonero N, Li W, Cabeza-Morales M, et al. New hope for pancreatic ductal adenocarcinoma treatment targeting endoplasmic reticulum stress response: a systematic review. *Int J Mol Sci*. 2018;19(9):2468. doi:10.3390/ijms19092468
42. Li SJ, Ding ST, Mersmann HJ, et al. A nutritional nonalcoholic steatohepatitis minipig model. *J Nutr Biochem*. 2016;28:51–60. doi:10.1016/j.jnutbio.2015.09.029
43. Zhang M, Liu X, Wang Q, et al. NDRG2 acts as a PERK co-factor to facilitate PERK branch and ERS-induced cell death. *FEBS Lett*. 2017;591(21):3670–3681. doi:10.1002/1873-3468.12861
44. Ibrahim IM, Abdelmalek DH, Elfiky AA. GRP78: a cell's response to stress. *Life Sci*. 2019;226:156–163. doi:10.1016/j.lfs.2019.04.022
45. Dong J, Chen L, Ye F, et al. Mic19 depletion impairs endoplasmic reticulum-mitochondrial contacts and mitochondrial lipid metabolism and triggers liver disease. *Nat Commun*. 2024;15(1):168. doi:10.1038/s41467-023-44057-6
46. Qian H, Chao X, Williams J, et al. Autophagy in liver diseases: a review. *Mol Aspect Med*. 2021;82:100973. doi:10.1016/j.mam.2021.100973
47. Sarabhai T, Kahl S, Gancheva S, et al. Loss of mitochondrial adaptation associates with deterioration of mitochondrial turnover and structure in metabolic dysfunction-associated steatotic liver disease. *Metabolism*. 2024;151:155762. doi:10.1016/j.metabol.2023.155762
48. Chen J, Jian L, Guo Y, et al. Liver cell mitophagy in metabolic dysfunction-associated steatotic liver disease and liver fibrosis. *Antioxidants*. 2024;13(6):729. doi:10.3390/antiox13060729
49. Lazarou M, Sliter DA, Kane LA, et al. The ubiquitin kinase PINK1 recruits autophagy receptors to induce mitophagy. *Nature*. 2015;524(7565):309–314. doi:10.1038/nature14893
50. Pierantonelli I, Svegliati-Baroni G. Nonalcoholic fatty liver disease: basic pathogenetic mechanisms in the progression from NAFLD to NASH. *Transplantation*. 2019;103(1):e1–e13. doi:10.1097/TP.0000000000002480
51. Park GC, Bang SY, Kim JM, et al. Inhibiting ferroptosis prevents the progression of steatotic liver disease in obese mice. *Antioxidants*. 2024;13(11):1336. doi:10.3390/antiox13111336
52. Li J, Cao F, Yin HL, et al. Ferroptosis: past, present and future. *Cell Death Dis*. 2020;11(2):88. doi:10.1038/s41419-020-2298-2
53. Im GY, Asgharpour A, Aby ES, et al. Medications for weight loss and MASLD: a national survey of hepatology and gastroenterology provider practices, attitudes, and knowledge before resmetirom. *J Clin Gastroenterol*. 2025. doi:10.1097/MCG.0000000000002147
54. Garvey WT, Batterham RL, Bhatta M, et al. Two-year effects of semaglutide in adults with overweight or obesity: the STEP 5 trial. *Nat Med*. 2022;28(10):2083–2091. doi:10.1038/s41591-022-02026-4